CHAPTER III

Studies on a new Schiff base ligand $H_3(pte_2\text{-}tsc)$ synthesized by condensing 7 – acetonyl – xanthopterin $[H_2(pte_2)]$ with thiosemicarbazide [H(tsc)] and its molybdenum complexes exhibiting reactivity towards $Me_3N\rightarrow O$, $PyN\rightarrow O$ and PPh_3 ; crystal structure of 2 – pivaloylamino – 7 – acetonyl–xanthopterin – water (1/1).

Abstract

A new Schiff base ligand $H_3(pte_2\text{-}tsc)$ (**1**) was synthesized by the condensation of 7-acetonyl-xanthopterin [$H_2(pte_2)$] and thiosemicarbazide [H(tsc)]. The pterin starting material obtained by modifying a published method, was characterized through single crystal X-ray diffraction analysis of its 2-pivaloylamino derivative and other data; they are consistent with its 7-substituted-xanthopterin representation. Six new Mo(IV,V,VI) complexes have been synthesized using this Schiff base ligand and characterized by different physico-chemical methods including elemental analysis, ESIMS, Λ_M data, ^1H NMR, IR, UV-VIS, fluorescence spectroscopy, CV data and supported by CHEM3D representations with lowest steric energy MM2 calculation. Here the $H_3(pte_2\text{-}tsc)$ ligand acts as a reducing agent, reducing the metal centre of the molybdenum starting materials to some lower oxidation states ($Mo^{IV/V}$) during synthesis in most cases. These complexes show reactivity towards oxygen atom donor agents, e.g., $Me_3N\rightarrow O$ or $PyN\rightarrow O$ and kinetics of these reactions have been studied. For compound (**4**), which was obtained as oxidized product (Mo^{VI} center) by the aerial oxidation of (**3**), shows reactivity towards a typical oxygen atom abstractor, like PPh_3. All these reactions have negative values for entropy of activation [$\Delta S^{\#}$ = (– 198 to – 208) J mol^{-1} deg^{-1}], suggesting associative type reaction mechanism, like the enzyme-substrate reactions. These kinetic data [e.g., k_{obs} = (3.82 x 10^{-3} – 80.00 x 10^{-3}) s^{-1}] are at par with the available literature in the related fields.

In several cases the reactivity aspects have been substantiated by kinetic data as well as reaction stoichiometry studies. They throw light on the oxidation state of the molybdenum centre in the pertinent compounds. Fluorescence spectral data give information on the changes in electron density on the complex during reaction with oxygen donor ($Me_3N\rightarrow O$) or oxygen abstractor (PPh_3) reagents. CV data indicate that the ligand centred redox process is considerably modified through coordination to the molybdenum centre.

Introduction

Considering the composition of the metal centered functional unit (McFU) of oxomolybdoenzymes [1, 2], this Chapter embodies the synthesis of a new ligand, $H_3(pte_2$-tsc), its corresponding molybdenum complexes as well as their reactivity, especially towards the relevant enzyme substrates. This new ligand [Scheme (III–1A)] was synthesized by condensing a 7–substituted pterin [7–acetonyl–xanthopterin, $H_2(pte_2)$] with thiosemicarbazide [H(tsc)]. Scheme (III–1B) reflects another tautomeric form of this ligand involving the thiocarbonyl group (S = C <) and NH_2 (γ) as well as the NH(3) and O(4) amide functions :

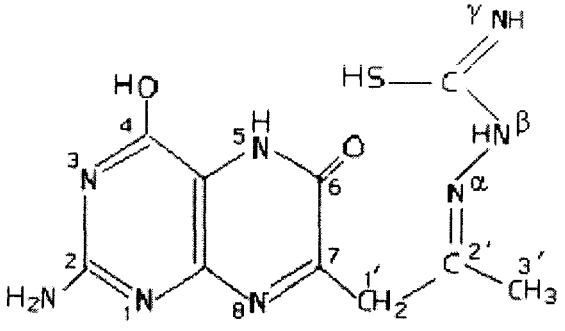

Scheme (III – 1A)

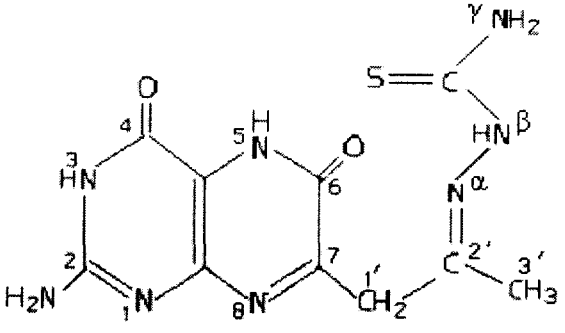

Scheme (III – 1B)

Scheme (III – 1)

All attempts for obtaining a similar Schiff base derivative with thiosemicarbazide through condensation with 6–acetonyl–isoxanthopterin [$H_2(pte_1)$] led to a cyclised product with no free metal coordination site. Distinct chemical difference between the two pterin starting materials, is responsible for the failure of $H_2(pte_1)$ in furnishing a suitable Schiff base ligand. Most likely the higher basicity of the NH(5) site, along with tautomerism with the 6 – substituent, [Scheme (II-1)] is responsible for the above observation i.e., formation of a cyclised product with thiosemicarbazide in case of $H_2(pte_1)$.

As far as this Schiff base ligand [$H_3(pte_2\text{-tsc})$] is concerned there are three possible deprotonation sites e.g., OH(4), NH(5) and the thiol group [Scheme (III-1A) & Scheme (III-1B)]. Actual state of protonation of the ligand residue in complex compounds depends on several factors e.g., reaction conditions, oxidation state of the metal centre, presence of secondary ligands etc. This has been ascertained here through different physico-chemical and spectroscopic methods including IR and ^1H NMR spectra as well as molecular modeling studies (e.g., the CHEM3D model giving the lowest steric energy through MM2 calculations, among different alternatives). As stated at the outset (Chapter I), the optimized bond length and bond angle data of the present systems have been compared with the literature X – ray structural data of related systems for authentication.

For confirming the structure of 7–acetonyl–xanthopterin, its 2–pivaloylamino substituted derivative was obtained through reaction with pivalic anhydride and it could be crystallized out [CH_3OH – CH_2Cl_2 (1:1,v/v)] for obtaining single crystals suitable for X-ray structure determination. It has distinctly higher solubility in the crystallizing solvent [CH_3OH – CH_2Cl_2 (1:1,v/v)] as compared to the unpivalated ligand due to hydrogen bonding involving its $NH_2(2)$ group [Scheme (P-1)] [125]. The notable aspect of the stability of the hydrogen bond between the pterin ligand and its constituent water molecule in (**a**) {[H_2(2-piv-pte$_2$)].H_2O} is verified through single crystal X-ray structure determination of 2-pivaloylamino-7-acetonyl-xanthopterin monohydrate. Here the H_2O molecule is bonded to the NH(2) group [as per Fig.(III – 1A) the N(2) – H --- O hydrogen

bonding distance is 2.945 Å]. This strongly hydrogen bonded H_2O molecule is not removed even during the reaction of 7-acetonyl-xanthopterin with pivalic anhydride. This pivalated pterin $[H_2(2\text{-piv-pte}_2)].H_2O$ was characterized by other physico-chemical methods (e.g., elemental analysis, ESIMS data, IR, UV-VIS, ^1H NMR spectra etc.), in addition to its single crystal X-ray structure determination.

In the next part of this chapter, chelating property of this N,O,S – donor Schiff base ligand [Scheme (III-1A) & Scheme (III-1B)] towards different molybdenum starting materials, characterization of the resulting complexes isolated in the solid state as well as their reactivity aspects are delineated.

Experimental

Materials: Reagent grade chemicals were used as received. Solvents were purified before use following literature procedures [9]. Kinetic and electrochemical studies were performed in spectroscopy grade DMF(SRL, Mumbai). Bu_4NClO_4 (TBAP) and PyN→O were prepared following literature procedures [7, 10, 11]. $Me_3N\rightarrow O$ was obtained from Aldrich, Mumbai. 7-acetonyl-xanthopterin monohydrate $[H_2(pte_2)].H_2O$ was prepared in this laboratory and characterized through X-ray crystallography using a single crystal of its pivalated derivative. It was obtained by a similar method as that for 6-acetonyl-isoxanthopterin $[H_2(pte_1]$ discussed in Chapter II except maintaining the pH at lower range (pH 4 – 4.5)[6]. Thiosemicarbazide and PPh_3 were obtained from SRL, Mumbai. $MoO_2(acac)_2$, $(Et_4N)_2[MoOCl_5]$, $MoOCl_3(bipy)$, $(Et_4N)_2[MoS_4]$ and $(Bu_4N)_4[Mo_8O_{26}]$ were prepared in this laboratory following published methods [40].

Method: All synthetic steps were carried out under dinitrogen atmosphere by applying Schlenk technique, except compound (4). For maintaining the desired reaction temperature, a silicon oil bath was used. Most of the physico-chemical methods are stated in Chapter II, Section – I. ^1H NMR data were obtained from R.S.I.C., Lucknow (300 MHz, DRX). IR data (KBr) were recorded in Shimadzu FTIR 8300. Steric energy

calculation of the CHEM3D representations were performed in CHEM3D Ultra, Version 8.0 (2004), Cambridge Soft Corporation, USA and the relevant structures were drawn in the higher versions. The UV-VIS absorption spectral monitoring of the reactions of the compounds with typical enzyme substrates like $PyN\rightarrow O$, $Me_3N\rightarrow O$ or PPh_3 were carried out for throwing light on the oxidation state of the metal centre in these compounds. Kinetics of these reactions in DMF were followed under pseudo-first order condition (maintaining 35-70 times excess of the substrate, $PyN\rightarrow O$, $Me_3N\rightarrow O$ / PPh_3). Rate constants (k_{obs}) were calculated from the plots of $\log(A_t-A_\infty)$ or $\log(A_\infty-A_t)$ vs. time, which were linear for at least three half-lives [8(a,c), 17, 23].

X – ray data collection and reduction

A red coloured monoclinic crystal of H_2(2-piv-pte$_2$).H_2O (**a**) was obtained by slow evaporation of CH_3OH – CH_2Cl_2 (1:1,v/v) solution of (**a**) over silica-gel in a desicator for 10 days in darkness. This crystal was used for single crystal X-ray diffraction study at the SAIF, Madras as a paid technical service; an Enraf Nonius CAD 4 automatic diffractometer was used for this purpose and the basic conditions are stated in Table (III–1). The ORTEP diagram is shown in Fig.[III–1(A)] and the unit cell structure showing hydrogen bonding in different layers are presented in Fig.[III–1(B)] and Table (III – 3). Table (III – 4) shows the atomic coordinates (x 10 ^ 4) and equivalent isotropic displacement parameters (A^ 2 x 10 ^ 3) for (**a**). Table (III – 5) displays the anisotropic displacement parameters (A ^ 2 x 10 ^ 3). Hydrogen coordinates (x 10 ^ 4) and isotropic displacement parameters (A ^ 2 x 10 ^ 3) are presented in Table (III – 6) and the torsion angles [deg.] are given in Table (III – 7).

Synthesis of compounds

H_2(2-piv-pte$_2$).H_2O (a)

7 – acetonyl-xanthopterin [H_2(pte$_2$)].H_2O (2.0 g, 7.9 mmol) and pivalic anhydride [($Me_3CCO)_2O$] (3.213 g, 10.072 mmol, 3.5 ml) was taken in a 25 ml round bottomed flask and fitted with a micro condenser. The mass was subjected to reflux in an oil bath under dinitrogen atmosphere and darkness for 3 h. A deep brown solution was formed which on concentration in a rotary evaporator at 343 K a brown residue was obtained. This was subjected to high pressure coloumn chromatography (silica-gel, 400 mesh). The fraction in CH_2Cl_2 was collected as a dark brown solution and concentrated in rotary evaporator to get a dirty – brown solid which was dried in vacuo over silica-gel for 48 h. Yield: 70%. This compound has high solubility in CH_2Cl_2, $CHCl_3$, CH_3OH etc. Purity of the product was checked through TLC [Silica-gel GF_{254} ; I_2 – chamber], using CH_2Cl_2 solution and diethyl ether as eluant. R_f.: 0.62. Found : C, 53.7; H, 6.4; N, 19.9 %. Calc. for $C_{14}H_{19}N_5O_5$: C, 49.9; H, 5.6; N, 20.8 %. UV-VIS absorption bands [CH_3OH, λ_{max}^{nm}(logϵ)]: 221 (4.06); 239 sh(3.89); 293 (3.74); 307 (3.72); 321 sh(3.73); 338 sh(3.80); 353 (3.82); 413 (3.62); 441 sh(3.37).

H_3(pte$_2$ -tsc). DMF (1)

A DMF solution (110 ml) of 7-acetonyl-xanthopterin monohydrate, [H_2(pte$_2$)].H_2O (0.253 g, 1 mmol) and a methanolic solution (10 ml) of sodium acetate (anhydrous) (0.123 g, 1.5 mmol) was mixed together in a flask and stirred for 5 min. A solution of thiosemicarbazide H(tsc) (0.091 g, 1 mmol) in DMF (40 ml) was added to the above reaction mixture. Within 10 min. the solution turned greenish-yellow with a flocullant precipitate; stirring at 343-353K under dinitrogen atmosphere and darkness, was continued for 1 h. After settling for 10 min., the reaction mixture was evaporated in rotary evaporator at 343K. The reddish-yellow residue was triturated with CH_3OH (5 ml) and then diethyl ether was added. The reddish-brown crystalline precipitate so obtained was filtered using a glass-fritte, washed with CH_3OH, ether and dried in vacuo over

silica-gel. Yield: 85%. Its solubility is ca. 4% in DMSO (warming and stirring) and slightly lower in DMF. Purity of the product was checked through TLC [Silica-gel GF_{254}; UV-chamber], using DMSO solution (diluted with 100 times CH_3OH) and CH_2Cl_2-$CHCl_3$ (1:1, v/v) as eluant. R_f.: 0.44. Found : C, 40.5; H, 5.0; N, 32.7; S, 8.2 %. Calc. for $C_{13}H_{19}N_9O_3S$: C, 40.9; H, 4.9; N, 33.1; S, 8.4 %. UV-VIS. absorption bands [DMF, $\lambda_{max}^{nm}(\log\epsilon)$]: 310 (2.12); 355.5 sh (1.90); 408 br (2.02).

$[Mo^{IV}(pte_2\text{-}tsc)(OCH_3)(CH_3OH)].0.5CH_3OH$ (2)

To a DMF solution (100 ml) of $[Mo^{VI}O_2(acac)_2]$ (0.326 g, 1 mmol), another solution (in DMF,100 ml) of the ligand, $H_3(pte_2\text{-}tsc)$.DMF, (0.381 g, 1 mmol) was mixed in a Schlenk flask. Heating and stirring at 313-323K under dinitrogen atmosphere and darkness was continued for 3 h. The yellow solution formed was allowed to settle for 1 h. The solvent was removed in rotary evaporator at 343K. The red oily residue formed was triturated with CH_3OH (15 ml); diethyl ether (10 ml) was added when a red crystalline precipitate was obtained. It was filtered under dinitrogen, in a glass-fritte, washed with CH_3OH, diethyl ether and dried in vacuo over silica - gel. Yield: 65%. Its solubility is ca. 5.5% in DMF. Purity of the product was checked through TLC [Silica-gel GF_{254} ; UV-lamp], using DMSO solution (diluted with 100 times CH_3OH) and CH_2Cl_2 as eluant. R_f : 0.46. Found : C, 29.0; H, 3.6; N, 23.0; S, 6.9; Mo, 20.1 %. Calc. for $MoC_{12.5}H_{18}N_8O_{4.5}S$: C, 31.2; H, 3.8; N, 23.3; S, 6.7; Mo, 20.0 %. UV-VIS absorption bands [DMF, $\lambda_{max}^{nm}(\log\epsilon)$]: 285(3.95); 341(4.02); 398(3.69); 420(3.68); 453sh (3.47). The compound is found to be diamagnetic in nature.

$[Mo^{IV}\{H(pte_2\text{-}tsc)\}Cl_2.DMF]$. 2DMF (3)

A DMF solution (20 ml) of $(Et_4N)_2[Mo^{V}OCl_5]$ (0.55 g, 1 mmol) was mixed with a solution of $H_3(pte_2\text{-}tsc)$.DMF (0.381 g, 1 mmol) in DMF (100 ml) in a Schlenk flask. The solvent and solutions were initially purged thoroughly with dinitrogen before mixing. Heating and stirring at 333K under dinitrogen atmosphere, darkness, was continued for 3h. A dark-red solution so obtained was concentrated to a red oil in rotary evaporator at

343K. This on trituration with CH_3OH (10 ml) yielded a red crystalline precipitate, filtered in a glass-fritte, washed with CH_3OH, diethyl ether and dried in vacuo over silica-gel. Yield: 60 %. Its solubility is ca. 5% in DMF. It's purity was checked through TLC [Silica-gel GF_{254}; UV-lamp], using DMSO solution (diluted with 100 times CH_3OH) and diethyl ether as eluant. R_f : 0.25. Found : C, 33.5; H, 4.1; N, 22.2; S, 4.6; Mo, 14.1%. Calc. for $MoC_{19}H_{31}N_{11}O_5SCl_2$: C, 33.0; H, 4.5; N, 22.2; S, 4.6; Mo, 13.9 %. UV-VIS absorption bands [DMF, $\lambda_{max}^{nm}(\log\epsilon)$]: 291(4.37); 346(4.45); 396(4.26); 420 sh(4.19); 453 sh(3.93). The compound is found to be diamagnetic in nature.

$(Et_4N)[(Mo_2^{VI}O_3)\ \{H(pte_2\text{-}tsc)\}Cl_5].\ 0.5CH_3OH$ (4)

This compound was prepared from (**3**) stated above in the following way : after removing solvent (DMF) in rotary evaporator from the reaction mixture of (**3**) at 343K, a red oily mass so obtained was allowed to attain room temperature (301K); sufficient amount of CH_3OH was added to have a clear solution. This solution was left in contact of air at 301K for 50h, during which the initial red colour changed slowly to green, concentrated to a minimum volume (5 ml) in a rotary evaporator when a green coloured precipitate settled down, filtered in a glass-fritte, washed with CH_3OH, diethyl ether and dried in vacuo over silica-gel. Yield: 62%. Its solubility is ca. 5% in DMF. Purity of the product was checked through TLC [Silica-gel GF_{254} ; UV-lamp], using diluted (with 100 times CH_3OH) DMSO solution and CH_2Cl_2 as eluant. R_f : 0.35. Found : C, 25.5; H, 3.6; N, 14.3; S, 4.0; Mo, 22.0 %. Calc. for $Mo_2C_{18.5}H_{32}N_9O_{5.5}Cl_5S$: C, 25.5; H, 3.7; N, 14.5; S, 3.7; Mo, 22.1%. UV-VIS absorption bands [DMF, $\lambda_{max}^{nm}(\log\epsilon)$]: 291(4.00); 341(4.05); 396 sh(3.75); 419 sh(3.68); 453(3.44). The compound is diamagnetic in nature.

$[(Mo_2^{V}O)_2\ \{H(pte_2\text{-}tsc)\}_2(bipy)Cl_{12}].\ 8CH_3OH$ (5)

A DMF solution (80 ml) of $[Mo^{V}OCl_3(bipy)]$ (0.374 g, 1 mmol) was charged with another DMF (100 ml) solution of $H_3(pte_2\text{-}tsc)$.DMF (0.381 g, 1 mmol) and subjected to heating (at 333K) and stirring under dinitrogen atmosphere, darkness, for 3h. A clear red solution was obtained, concentrated in rotary evaporator at 343K when a red oil was

formed. On trituration with CH_3OH (10 ml) gave a brick-red coloured, air stable precipitate which was filtered in a glass-fritte and dried in vacuo over silica-gel. Yield: 65%. Solubility of the complex is ca. 5.5 % in DMF. Purity of this compound was checked through TLC [Silica-gel GF_{254} ;I_2-chamber], using DMSO solution (diluted with 100 times CH_3OH) and CH_2Cl_2 as eluant. R_f : 0.40. Found : C, 23.2; H, 2.8; N, 12.5; S, 4.0; 20.7 %. Calc. for $Mo_4C_{38}H_{60}N_{18}O_{14}Cl_{12}S_2$: C, 24.4; H, 3.2; N, 13.5; S, 3.4; Mo, 20.6 %. UV-VIS absorption bands [DMF, $\lambda_{max}^{nm}(\log\epsilon)$]: 281.7(4.74); 343.6(4.52); 398 br(4.18); 422(4.18); 453(4.08); 491 sh(3.84). The compound is found to be diamagnetic in nature.

$[(Mo_2^{V}O_4)\ \{H(pte_2\text{-}tsc)\}\ (DMF)_3].DMF.CH_3OH$ (6)

To a DMF solution (80 ml) of $(Bu_4N)_4[Mo_8^{VI}O_{26}]$ (269 g, ⅛ mmol) in a Schlenk flask, $H_3(pte_2\text{-}tsc).DMF$ (0.381 g, 1 mmol) in DMF (100 ml) was added under dinitrogen atmosphere. Heating and stirring of the reaction mixture at 338K under dinitrogen atmosphere and darkness was continued for 2h. The reaction mixture turned deep greenish-yellow. The solvent was removed in rotary evaporator at 343K when a brownish, oily residue was formed which on trituration with CH_3OH (10 ml) a green precipitate formed. This was filtered in a glass-fritte and washed with CH_3OH, diethyl ether; dried in vacuo over silica-gel. Yield: 60%. Its solubility is ca. 5% in DMF. Purity of the compound was checked through TLC [Silica-gel GF_{254} ;UV-chamber], using DMSO solution (diluted with 100 times CH_3OH) and CH_2Cl_2 as eluant. R_f : 0.50. Found : C, 32.1; H, 4.2; N, 18.5; S, 3.7; Mo, 21.8 %. Calc. for $Mo_2C_{23}H_{42}N_{12}O_{11}S$: C, 31.1; H, 4.7; N, 18.9; S, 3.6; Mo, 21.7%. UV-VIS absorption bands [DMF, $\lambda_{max}^{nm}(\log\epsilon)$]: 279(4.28); 339(4.26); 422(3.86); 453 sh(3.77); 486 sh(3.49). The compound is diamagnetic in nature.

$[(Mo_2{}^{VI}S_5)\ \{H(pte_2\text{-}tsc)\}\ (CH_3OH)_3].CH_3OH$ (7)

To a methanolic solution (30 ml) of $(Et_4N)_2[MoS_4]$ (0.484 g, 1 mmol), taken in a three necked Schlenk flask, a DMF solution (100 ml) of $H_3(pte_2\text{-}tsc).DMF$ (0.381 g, 1 mmol) was charged slowly through an addition funnel under stirring at 301K. The pH of the reaction mixture was adjusted to 6.0 with HCl in dioxane. The resulted solution was stirred at 333K under dinitrogen atmosphere, darkness, for 2 h when a dark red coloured solution was formed. This was concentrated to an oily residue in a rotary evaporator at 343K and subsequently triturated with CH_3OH (5 ml) to get a pink-brown precipipate which was filtered in a glass-fritte, washed with CH_3OH, diethyl ether and dried in vacuo over silica-gel. Yield: 45%. Its solubility is ca. 4.5% in DMF. Purity of the product was checked through TLC [Silica-gel GF_{254} ;UV-chamber], using DMSO solution (diluted with 100 times CH_3OH) and CH_2Cl_2-$CHCl_3$ (2:1,v/v) solvent mixture as eluant. R_f : 0.33. Found : C, 21.9; H, 3.4; N, 13.7; S, 25.0; Mo, 24.3 %. Calc. for $Mo_2C_{14}H_{27}N_8O_6S_6$: C, 21.35; H, 3.43; N, 14.23; S, 24.4; Mo, 24.4 %. UV-VIS absorption bands [DMF, $\lambda_{max}{}^{nm}(log\epsilon)$]: 280.5(4.33); 340(4.30); 398 br(3.97); 420(3.97); 453 sh(3.82). The compound is found to be diamagnetic in nature.

Results and Discussion

The molecular structure of H_2(2-piv-pte$_2$).H_2O along with its numbering scheme is shown in Fig.[III–1(A)]. The data clearly shows the xanthopterin structure (7-oxo) of this Ligand [28]. Table (III–2) contains different bond lengths and bond angles information. The crystal contains one water molecule hydrogen bonded to the N(1) atom of the pterin as well as O(4) and N(5), as evident from Table (III – 3). The unit cell structure along with inter – layer hydrogen bonding is shown in Fig.[III – 1(B)].

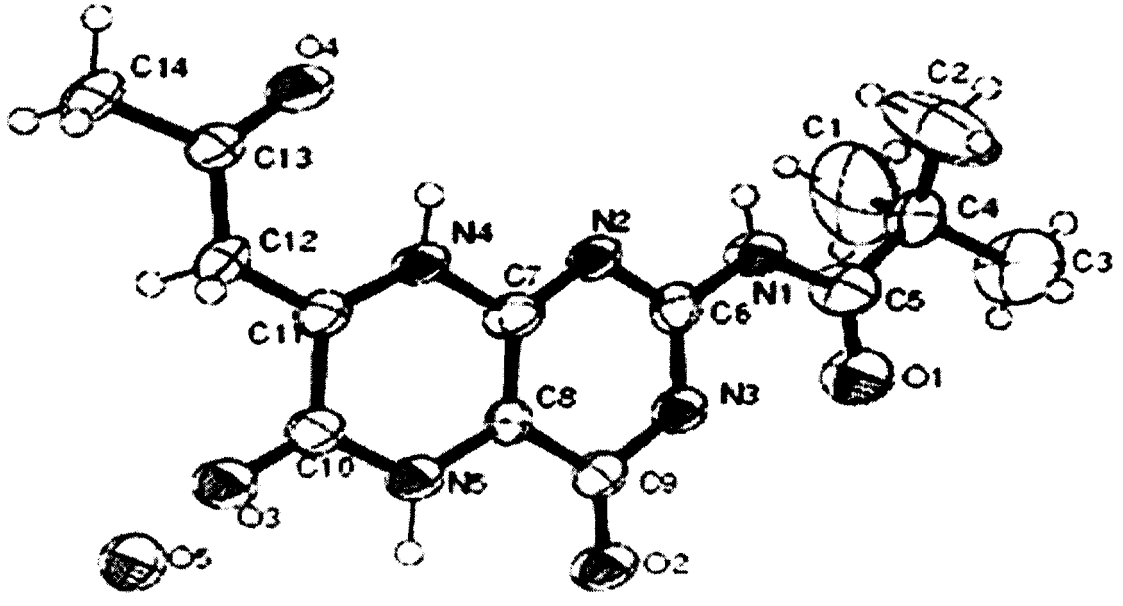

Fig. (III-1A)

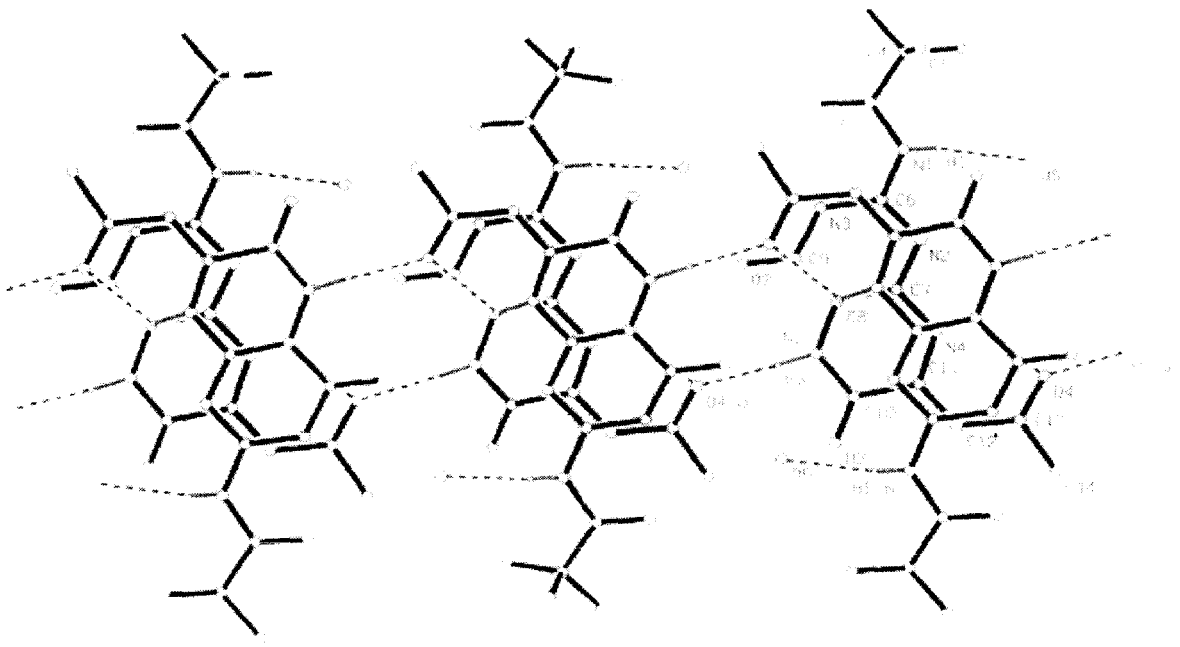

Fig. (III-1B)

Fig.(III–1): (A) represents the single crystal X–ray structure of H_2(2-piv-pte$_2$).H_2O molecule and (B) the unit cell structure of H_2(2-piv-pte$_2$).H_2O crystal.

Table (III – 1): Crystal data and structure refinement for H_2(2-piv-pte$_2$).H_2O:

Empirical formula	$C_{14}H_{19}N_5O_5$
Formula weight	337.34
Temperature	293(2) K
Wave length	0.71073 Å
Crystal system	Monoclinic
Space group	P21/a
Unit cell dimensions	a = 15.722(5) Å alpha = 90 deg.
	b = 6.598(4) Å beta =104.76(3) deg.
	c = 16.382(6) Å gamma = 90 deg.
Volume	1643.4(14) A^ 3
z	4
Calculated density	1.363 mg/ m^ 3

Absorption coefficient	0.105 mm^ -1
F(000)	712
Crystal size	0.3 x 0.2 x 0.2 mm
Theta range for data collection	2.57 to 24.96 deg.
Limiting indices	0 <= h <= 18, 0 <= k <= 7, -19 <= l <= 18
Reflections collected / unique	2980 / 2860 [R(int) = 0.0279]
Completeness to theta = 24.96	99.3 %
Absorption correction	Psi- scan
Max. and min. transmission	0.9972 and 0.9032
Refinement method	Full- matrix least- squares on F^2
Data / restraints / parameters	2860 / 0 / 230
Goodness- of- fit on F^2	0.847
Final R indices [I > 2 sigma(I)]	RI = 0.0572, wR2 = 0.1269
R indices (all data)	RI = 0.1869, wR2 = 0.1664
Extinction coefficient	0.0007(9)
Largest diff. peak and hole	0.250 and – 0.211 e. A^-3

Table (III – 2): Bond lengths [Å] and angles [deg.] for H_2(2-piv-pte$_2$) .H_2O # :

C(1) – C(4)	1.508 (9)	O(1)–C(5)– N(1)	118.8 (4)
C(2) – C(4)	1.477 (6)	O(1)–C(5)– C(4)	124.1 (4)
C(3) – C(4)	1.495 (6)	N(1)–C(5)– C(4)	117.0 (4)
C(4) – C(5)	1.485 (6)	N(2)–C(6)– N(1)	116.9 (3)
C(5) – O(1)	1.213 (4)	N(2)–C(6)– N(3)	123.2 (3)
C(5) – N(1)	1.397 (5)	N(1)–C(6)– N(3)	119.9 (3)
C(6) – N(2)	1.331 (4)	N(2)–C(7)– C(8)	126.3 (3)
C(6) – N(1)	1.365 (4)	N(2)–C(7)– N(4)	116.5 (3)
C(6) – N(3)	1.365 (4)	C(8)–C(7)– N(4)	117.2 (3)
C(7) – N(2)	1.344 (4)	C(7)–C(8)– N(5)	121.9 (3)
C(7) – C(8)	1.369 (5)	C(7)–C(8)– C(9)	118.5 (3)
C(7) – N(4)	1.393 (4)	N(5)–C(8)– C(9)	119.6 (3)

C(8) – N(5)	1.383 (4)	O(2)–C(9)– N(3)	122.2 (3)
C(8) – C(9)	1.443 (5)	O(2)–C(9)– C(8)	124.3 (4)
C(9) – O(2)	1.225 (4)	N(3)–C(9)– C(8)	113.5 (3)
C(9) – N(3)	1.389 (4)	O(3)–C(10) – N(5)	121.4 (3)
C(10) – O(3)	1.218 (4)	O(3) – C(10) – C(11)	122.8 (4)
C(10) – N(5)	1.360 (5)	N(5)–C(10)– C(11)	115.7 (3)
C(10) – C(11)	1.482 (5)	N(4)–C(11)– C(12)	123.5 (3)
C(11) – N(4)	1.352 (4)	N(4)–C(11)– C(10)	119.5 (3)
C(11) – C(12)	1.374 (5)	C(12)–C(11)– C(10)	117.0 (3)
C(12) – C(13)	1.417 (5)	C(11)–C(12)– C(13)	123.8 (4)
C(13) – O(4)	1.228 (4)	O(4)–C(13)– C(12)	122.5 (4)
C(13) – C(14)	1.529 (5)	O(4)–C(13)– C(14)	120.7 (3)
C(2)–C(4)– C(5)	114.6 (4)	C(12)–C(13)– C(14)	116.8 (3)
C(2)–C(4)– C(3)	111.4 (5)	C(6)–N(1)– C(5)	126.7 (3)
C(5)–C(4)– C(3)	107.6 (4)	C(6)–N(2)– C(7)	115.2 (3)
C(2)–C(4)– C(1)	109.0 (6)	C(6)–N(3)– C(9)	123.4 (3)
C(5)–C(4)– C(1)	106.3 (4)	C(11)–N(4)– C(7)	122.9 (3)
C(3)–C(4)– C(1)	107.6 (5)	C(10)–N(5)– C(8)	122.6 (3)

[#] Symmetry transformations used to generate equivalent atoms.

Table (III – 3): Hydrogen bonds for (**a**) [A and deg.] :

D – H . . . A	d (D – H)	d (H . . . A)	d (D . . . A)	< (DHA)
N(1) – H(1) . . . O(5) # 1	0.80 (3)	2.16 (3)	2.945 (4)	168 (3)
N(4) – H(4) . . . O(4)	0.89 (3)	2.13 (3)	2.687 (4)	120 (2)
N(5) – H(5) . . . O(4) # 2	0.95 (4)	1.92 (4)	2.870 (4)	178 (4)

Symmetry transformations used to generate equivalent atoms :
1 - x , - y +1, - z +1 # 2 x +1/2, - y +1/2, z

Table (III–4): Atomic coordinates (x 10 ^ 4) and equivalent isotropic displacement parameters (A^ 2 x 10 ^ 3) for (**a**). U(eq) is defined as one third of the trace of the orthogonalized Uij tensor.

	x	y	z	U(eq)
C(1)	751(6)	3866(13)	9080(4)	168(3)
C(2)	69(4)	552(14)	8780(3)	164(4)
C(3)	1624(3)	857(13)	9544(3)	150(3)
C(4)	893(3)	1696(9)	8857(3)	61(1)
C(5)	1204(3)	1768(7)	8074(3)	59(1)
C(6)	704(2)	2114(7)	6525(2)	43(1)
C(7)	161(2)	2447(7)	5116(2)	41(1)
C(8)	973(2)	2446(6)	4954(2)	40(1)
C(9)	1740(2)	2267(7)	5655(2)	47(1)
C(10)	383(2)	2927(7)	3461(3)	48(1)
C(11)	-500(2)	2839(7)	3626(2)	41(1)
C(12)	-1213(2)	3018(6)	2942(2)	40(1)
C(13)	-2098(2)	2956(7)	2996(3)	50(1)
C(14)	-2809(2)	3236(8)	2172(2)	73(2)
N(1)	563(2)	1974(6)	7311(2)	52(1)
N(2)	-5(2)	2276(5)	5879(2)	43(1)
N(3)	1542(2)	2090(5)	6431(2)	44(1)

N(4)	-568(2)	2594(6)	4427(2)	42(1)
N(5)	1075(2)	2644(6)	4144(2)	48(1)
O(1)	1970(2)	1672(6)	8061(2)	81(1)
O(2)	2499(2)	2270(5)	5588(2)	64(1)
O(3)	493(2)	3230(5)	2761(2)	64(1)
O(4)	-2297(2)	2696(5)	3666(2)	59(1)
O(5)	1307(2)	7106(5)	2859(2)	78(1)

Table (III–5) : Anisotropic displacement parameters (A ^ 2 x 10 ^ 3) for (**a**). The anisotropic displacement factor exponent takes the form :- 2 pi ^ 2 [h ^ 2 a * ^ 2 U11 + . . . + 2 h k a * b * U12]

	U11	U22	U33	U23	U13	U12
C(1)	262(10)	195(10)	64(4)	5(5)	71(5)	53(8)
C(2)	116(5)	316(12)	59(4)	2(5)	22(4)	-109(6)
C(3)	92(4)	299(10)	43(3)	42(5)	-13(3)	30(6)
C(4)	49(2)	92(5)	31(3)	4(3)	-8(2)	3(3)
C(5)	43(2)	84(4)	45(3)	-10(3)	0(2)	-16(3)
C(6)	42(2)	54(3)	28(2)	1(2)	3(2)	5(2)
C(7)	30(2)	52(3)	37(2)	-7(2)	3(2)	-1(2)
C(8)	31(2)	61(3)	24(2)	6(2)	2(2)	3(2)
C(9)	31(2)	63(3)	41(3)	3(2)	1(2)	- 4(2)

C(10)	32(2)	72(4)	37(2)	2(3)	5(2)	-1(2)
C(11)	31(2)	57(3)	32(2)	0(2)	3(2)	1(2)
C(12)	31(2)	44(3)	40(2)	3(2)	-1(2)	4(2)
C(13)	29(2)	79(4)	38(2)	8(3)	4(2)	0(2)
C(14)	28(2)	135(5)	45(3)	18(3)	-10(2)	4(3)
N(1)	28(2)	93(3)	29(2)	-1(2)	-1(2)	-3(2)
N(2)	28(2)	64(3)	35(2)	3(2)	2(2)	5(2)
N(3)	30(2)	58(3)	38(2)	1(2)	1(1)	1(2)
N(4)	21(2)	70(3)	32(2)	0(2)	-1(1)	0(2)
N(5)	27(2)	74(3)	40(2)	6(2)	4(2)	0(2)
O(1)	44(2)	143(4)	45(2)	13(2)	-6(2)	-5(2)
O(2)	26(1)	107(3)	52(2)	6(2)	1(1)	2(2)
O(3)	36(2)	113(3)	41(2)	10(2)	8(1)	1(2)
O(4)	28(1)	99(3)	49(2)	7(2)	6(1)	1(2)
O(5)	48(2)	133(3)	48(2)	8(2)	4(1)	-1(2)

Table (III – 6) : Hydrogen coordinates (x 10 ^ 4) and isotropic displacement parameters (A ^ 2 x 10 ^ 3) for (**a**).

	x	y	z	U(eq)
H(1A)	561	3902	9593	252
H(1B)	310	4473	8632	252
H(1C)	1292	4604	9158	252
H(2A)	- 80	555	9312	246
H(2B)	148	- 819	8617	246
H(2C)	- 396	1176	8359	246
H(3A)	1441	794	10060	226
H(3B)	2131	1718	9621	226
H(3C)	1770	- 480	9392	226
H(12A)	-1153	1958	2550	48
H(12B)	-1142	4294	2673	48
H(14A)	-3379	3161	2284	109
H(14B)	-2756	2189	1781	109
H(14C)	-2739	4536	1933	109
H(1)	60(20)	2090(50)	7314(19)	27(11)
H(4)	-1070(20)	2620(60)	4591(19)	39(10)
H(5)	1610(30)	2530(70)	3970(30)	72(13)

Table (III – 7) : Torsion angles [deg.] for (**a**) [#].

C(2) – C(4) – C(5) – (1)	- 141.9(6)
C(3) – C(4) – C(5) – O(1)	- 17.4(8)
C(1) – C(4) – C(5) – O(1)	97.6(6)
C(2) – C(4) – C(5) – N(1)	38.6(7)
C(3) – C(4) – C(5) – N(1)	163.1(5)
C(1) – C(4) – C(5) – N(1)	- 81.9(6)
N(2) – C(7) – C(8) – N(5)	- 179.6(4)
N(4) – C(7) – C(8) – N(5)	1.9(6)
N(2) – C(7) – C(8) – C(9)	- 0.6(7)
N(4) – C(7) – C(8) – C(9)	- 179.2(4)
C(7) – C(8) – C(9) – O(2)	- 179.2(5)
N(5) – C(8) – C(9) – O(2)	- 0.3(7)
C(7) – C(8) – C(9) – N(3)	0.7(6)
N(5) – C(8) – C(9) – N(3)	179.7(4)
O(3) – C(10) – C(11) – N(4)	- 176.8(4)
N(5) – C(10) – C(11) – N(4)	3.3(6)
O(3) – C(10) – C(11) – C(12)	3.1(7)
N(5) – C(10) – C(11) – C(12)	- 176.9(4)
N(4) – C(11) – C(12) – C(13)	- 0.4(7)
C(10) – C(11) – C(12) – C(13)	179.7(4)
C(11) – C(12) – C(13) – O(4)	-1.4(7)
C(11) – C(12) – C(13) – C(14)	178.5(4)
N(2) – C(6) – N(1) – C(5)	179.1(4)
N(3) – C(6) – N(1) – C(5)	-1.1(7)

O(1) – C(5) – N(1) – C(6)	-1.0(7)
C(4) – C(5) – N(1) – C(6)	178.5(5)
N(1) – C(6) – N(2) – C(7)	178.9(4)
N(3) – C(6) – N(2) – C(7)	- 0.9(6)
C(8) – C(7) – N(2) – C(6)	0.7(7)
N(4) – C(7) – N(2) – C(6)	179.2(4)
N(2) – C(6) – N(3) – C(9)	1.2(7)
N(1) – C(6) – N(3) – C(9)	-178.6(4)
O(2) – C(9) – N(3) – C(6)	179.0(4)
C(8) – C(9) – N(3) – C(6)	-1.0(6)
C(12) – C(11) – N(4) – C(7)	-178.9(4)
C(10) – C(11) – N(4) – C(7)	1.0(6)
N(2) – C(7) – N(4) – C(11)	177.8(4)
C(8) – C(7) – N(4) – C(11)	-3.5(6)
O(3) – C(10) – N(5) – C(8)	175.1(4)
C(11) – C(10) – N(5) – C(8)	- 4.9(6)
C(7) – C(8) – N(5) – C(10)	2.5(7)
C(9) – C(8) – N(5) – C(10)	- 176.4(4)

[#] Symmetry transformations used to generate equivalent atoms.

Fast Atomic Bombardment (FAB) / ESIMS technique, has proved to be a valuable tool for characterizing many compounds including the inorganic coordination ones[110, 121]. As is the case for different types of mass spectroscopy, the assignment of molecular formula (or any definite fragment originating from it) is confirmed by the experimental value of m/z (the most abundant isotopic mass) as well as matching

between the experimental and calculated (simulated) isotopic distribution profile [14, 85, 107, 117, 118]. As far as organic compounds containing O, F, P and I are concerned, the relative intensities of M, M+1 and M+2 isotope peaks are of great value in recognizing the molecular ion (M^+) peak or any well defined fragment confirming it [85]. Sometimes, isotope peaks may be more intense than the calculated values because of ion – molecule interactions that vary with the sample concentration or with the class of compound involved, e.g., the transfer of a hydrogen atom from the excess of the compound to the molecular ion in some case [85]. An M – 1 peak is common and occasionally an M – 2 peak (loss of H_2) or even a rare M – 3 peak (from alcohol) is reasonable [85]. Absence of molecular ion (or an extremely weak M^+ peak) is characteristic of highly branched molecules, alcohols, molecules with long alkyl chain, aryl ketones and benzyl compounds [85, 107].

FAB mass spectrum of (**1**) [Fig.(III–2)] contains the molecular ion peak without solvent molecule (DMF) of crystallization at m/z =307, $[M–DMF–H]^+$ (relative intensity 100%), where 'M' is the molecular formula of (**1**)[7(a), 14, 15, 85, 107] (F.W.= 381) This peak was simulated by IPC [46] [Fig.(III–3)]. The experimentally found peak and the simulated one show good agreement between them which supports the proposed molecular formula.

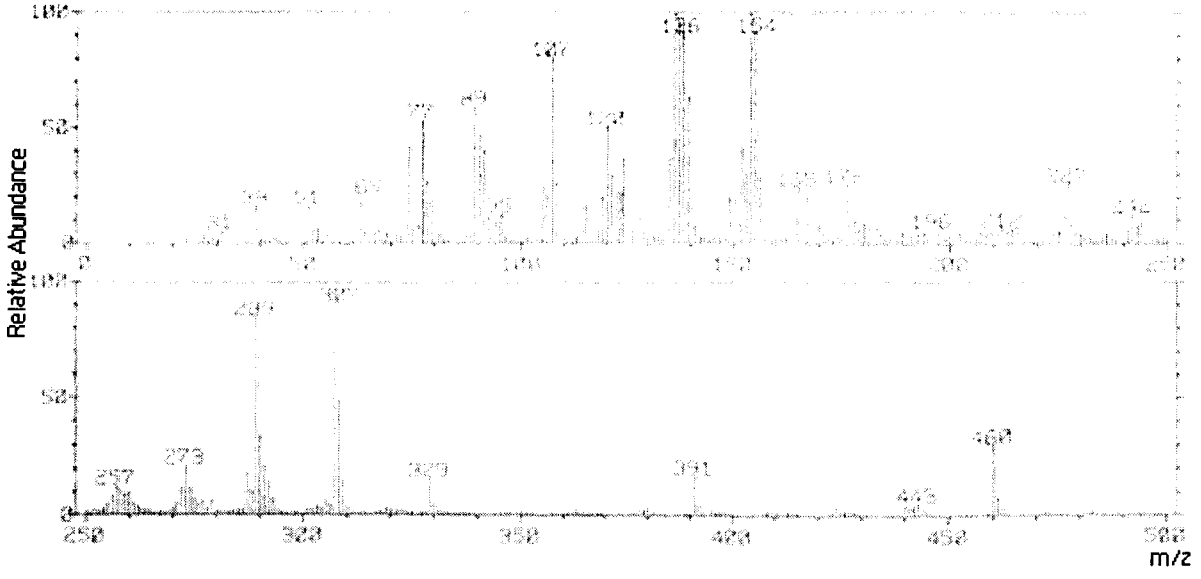

Fig.(III – 2): FAB Mass spectrum of (**1**) in CH_3OH.

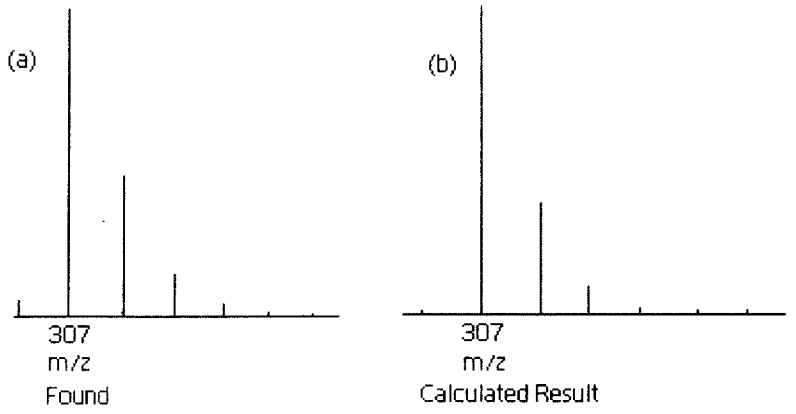

Fig.(III–3): (a) ESIMS data of (**1**) at the m/z (= 307) region corresponding to [M– DMF–H]$^+$; (b) the calculated isotope pattern [46]. Formula : $C_{10}H_{11}N_8O_2S$.

The desolvated molecular ion peak in the ESIMS spectrum of (**2**) appeared at m/z = 464, [M – 0.5CH_3OH]$^+$; where 'M' is the molecular formula of (**2**) (F.W.= 479.94)[7(a), 14, 15]. The molecular ion peak without 0.5CH_3OH is simulated [Fig.(III – 4)] by using the IPC program mentioned above[46]. Good agreement between the calculated and the experimentally found peaks suggests the correctness of the proposed molecular formula of (**2**).

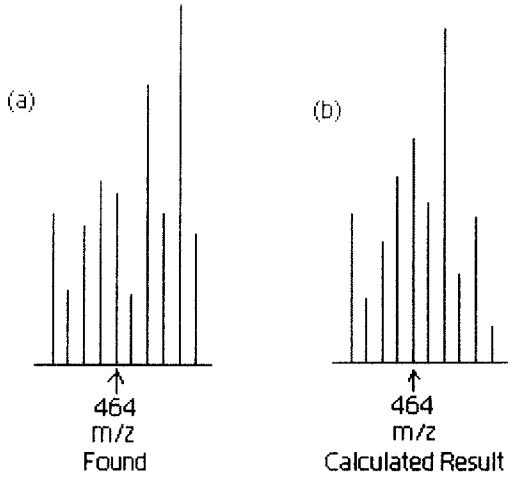

Fig.(III–4): (a) ESIMS data of (**2**) at the m/z (= 464) region corresponding to [M – 0.5CH_3OH]$^+$; (b) the calculated isotope pattern [46]. Formula :$C_{12}H_{16}N_8O_4MoS$.

In the ESIMS data of (**3**) the peak at m/z = 656 could be assigned to the characteristic fragment [M – Cl – 2H]$^+$ [85], where 'M' is the molecular formula of the complex (F.W.=692) [7(a), 14, 15]. The simulated and the experimentally obtained peaks

[Fig.(III – 5)] [14, 46] are consistent to each other and with the molecular formula of (**3**) [7(a), 14, 15, 85, 107].

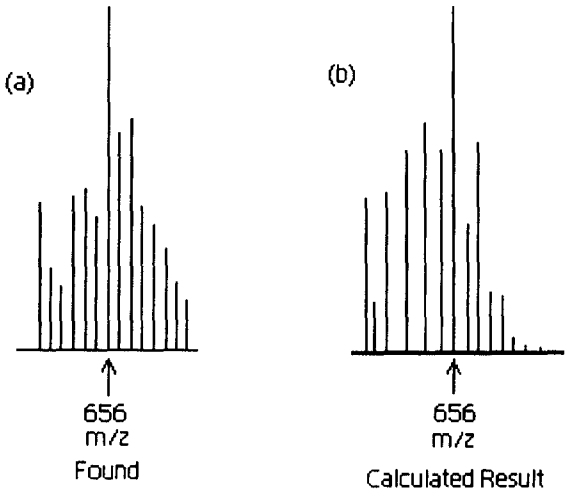

Fig.(III – 5): (a) ESIMS data of (**3**) at the m/z (= 656) region corresponding to [M – Cl – 2H]$^+$; (b) the calculated isotope pattern [46]. Formula :$C_{19}H_{29}N_{11}O_5MoSCl$.

The essentially desolvated ESIMS peak of (**4**) [M – 0.5CH_3OH – H]$^+$ is visible at m/z = 854, where 'M' is the molecular formula of the complex (F.W. = 869.38) [7(a), 14, 15, 85, 107]. This peak is simulated by using the IPC program [46] [Fig.(III – 6)] and found that both are in good match. The total number of peaks in this spectrum confirms the presence of a binuclear molybdenum species [14].

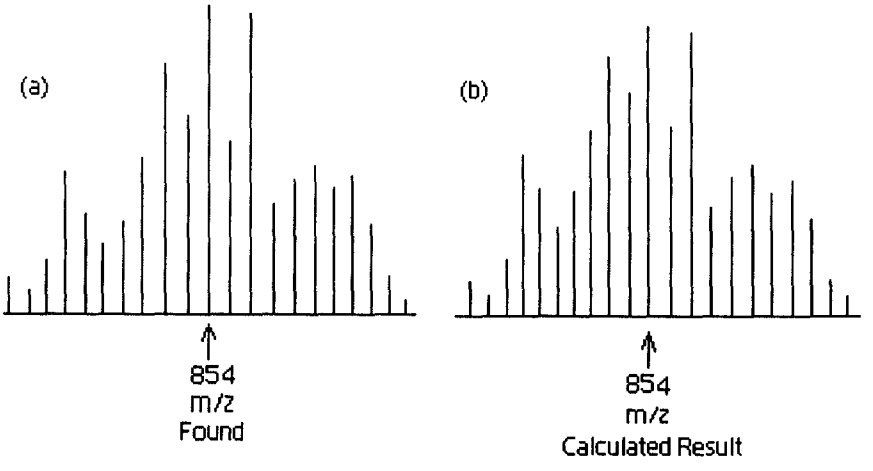

Fig.(III–6): (a) ESIMS data of (**4**) at the m/z (= 854) region corresponding to [M– 0.5CH_3OH – H]$^+$; (b) the calculated isotope pattern [46].Formula :$C_{18}H_{29}N_9O_5Mo_2Cl_5S$.

In case of (**5**) the ESIMS spectrum contains a peak at m/z = 894.3 which can be assigned to the fragment $[M/2 - Cl - 3H]^+$, where 'M' is the molecular formula of the compound (F.W.=1865.76.) [7(a), 14, 15]. [Fig.(III–7)][46] reflecting the matching of experimental and simulated ESIMS data confirms the binuclear nature of the fragment i.e., this in turn shows that the original tetranuclear species undergoes fragmentation process through a definite pathway leading to the above binuclear fragment [85, 107].

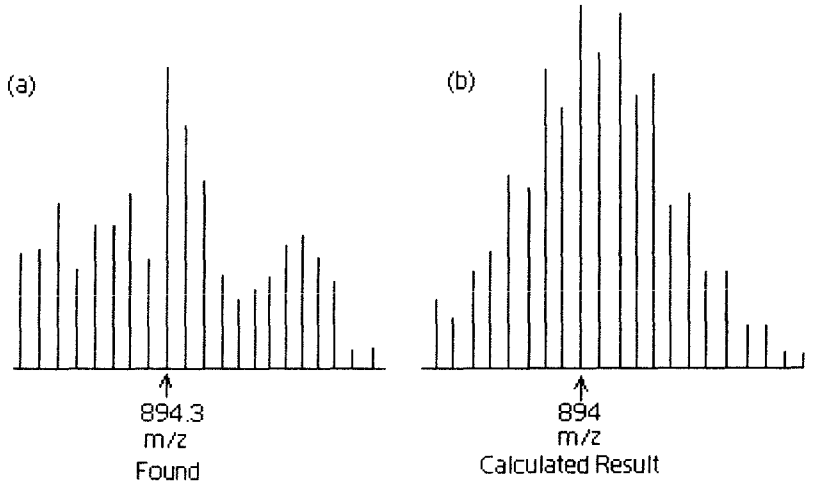

Fig.(III–7): (a) ESIMS data of (**5**) at the m/z (= 894.3) region corresponding to $[M/2 - Cl - 3H]^+$; (b) the calculated isotope pattern [46]. Formula : $C_{19}H_{27}N_9O_7Mo_2Cl_5S$.

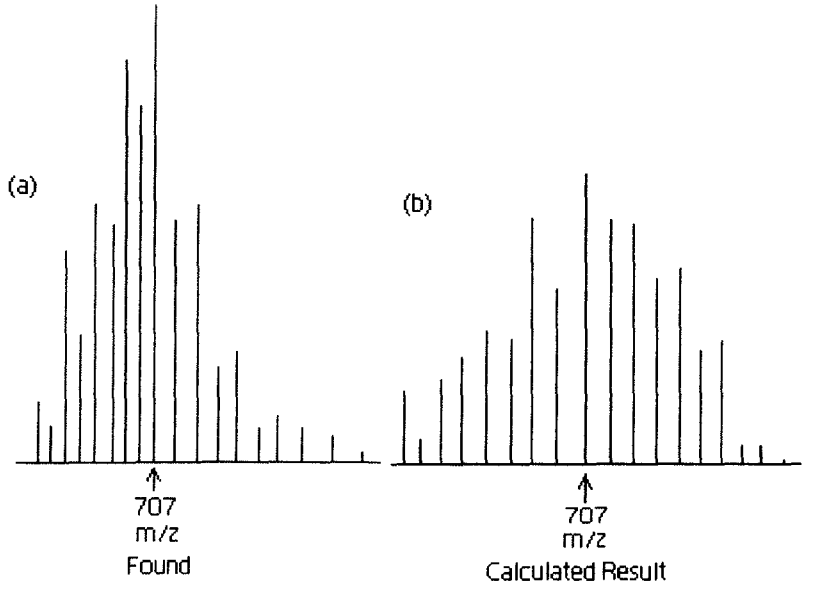

Fig.(III–8): (a) ESIMS data of (**6**) at the m/z (= 707.4) region corresponding to $[M - CH_3OH - 2DMF + H]^+$; (b) the calculated isotope pattern [46]. Formula :$C_{16}H_{23}N_{10}O_8Mo_2S$.

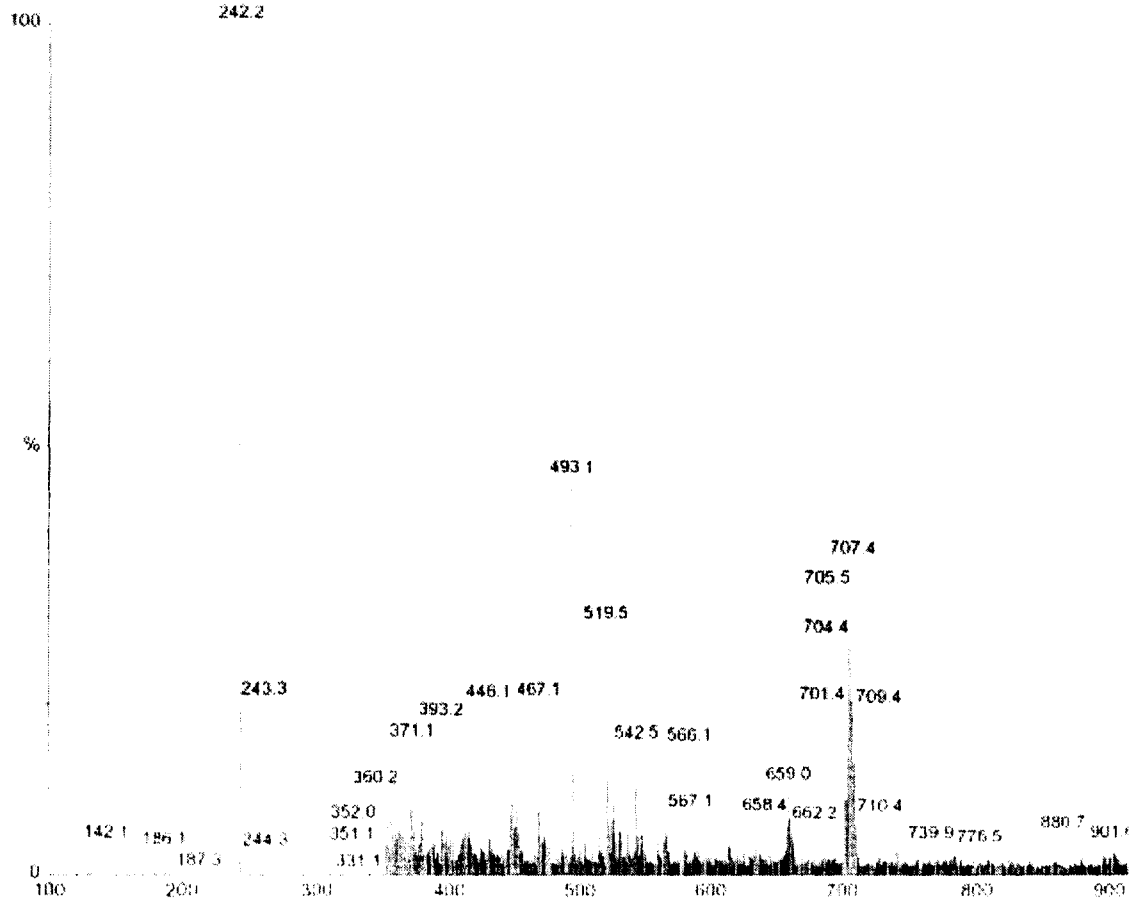

Fig.(III – 9): ESIMS spectrum of (**6**) in CH_3OH.

Compound (**6**) shows the ESIMS peak for the partly desolvated species $[M - CH_3OH - 2DMF - H]^+$ at m/z = 707.4, where 'M' is the relevant molecular formula (F.W. = 885.88)[7(a), 14, 15]. [Fig.(III – 9)] shows the ESIMS spectrum of (**6**), whereas [Fig.(III–8)] shows the simulated and experimental patterns for the above mentioned peak[46]. It is consistent with the binuclear formula of the complex [14].

In case of (7) the ESIMS data shows a fragment $[M - CO + H]^+$ at m/z = 760. It matches with its simulated pattern[14, 46] [Fig.(III–10)] thereby verifying the chemical composition of this compound.

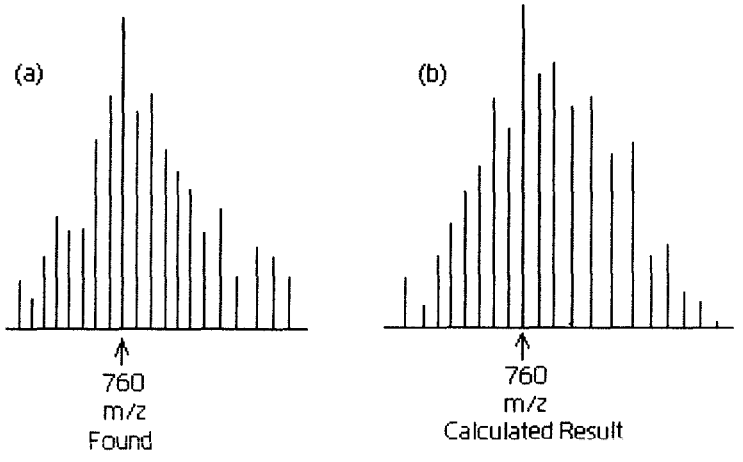

Fig.(III–10): (a) Computer simulation and (b) experimentally found ESIMS peaks of (7) corresponding to m/z = 760,$[M - CO + H]^+$. Formula : $C_{13}H_{28}N_8O_5Mo_2S_6$.

ESIMS method plays an important role in characterizing and identifying the novel products formed during its recording time [12]. In most of the cases discussed above, either the essentially almost intact molecular ion or the desolvated species could be assigned through matching of the relevant experimental and calculated isotopic distribution patterns. In a number of cases, definite fragments like a chlorine atom or a CO molecule is lost during the mass spectral process. These ESIMS data together with the elemental analysis data are adequate in establishing the chemical compositions of these new complexes described in the earlier part of this Chapter. The following peaks are found to be common in almost all the complexes discussed above: m/z = 331.1 $[Mo\{H_2(pte_2)\}]^+$; m/z = 307.1, $[H_2(pte_2\text{-}tsc)]^+$.

From the above discussion it is evident that the new Schiff base ligand, $H_3(pte_2\text{-}tsc)$ is a stable one and is able to retain its identity throughout its reactions with a variety of molybdenum starting materials, leading to pure products.

The Λ_M [(9.12 – 32.2) $ohm^{-1}\,cm^2\,mol^{-1}$, 301K, CH_3OH)] values for complexes **(2)**, **(3)**, **(5)**, **(6)** & **(7)** support the non-electrolytic formulation of these complexes[43]. In case of **(4)**, Λ_M (80.9 ohm^{-1} cm^2 mol^{-1}, 301K, CH_3OH) is consistent with the 1:1 electrolytic nature of this complex [43].

Some useful inferences regarding the ligand coordination sites could be drawn from a comparison of IR spectra of $[H_2(pte_2)]$, $H_3(pte_2\text{–}tsc)$ and the different complexes (**2** – **7**). Two intense bands with fine structure at 1690 cm^{-1} and 1650 cm^{-1} of $H_2(pte_2)$ corresponding to different types of ν (C=O) modes, are replaced by a band at 1647 cm^{-1} in (**1**) corresponding to ν (C=O) of O(6) and ν (C=N) of C(2′) [Scheme (III - 1)]. These two bands are present in slightly modified form in most of these complexes. As per X – ray structural data on different metal – pterin complexes [3, 18, 20, 39], the M – N(5) bond plays a pivotal role in the pterin ligand chelation process. Again in the free ligand (**1**), [Scheme (III – 1)] the ν(C – O) and ν(C– O) + δ(OH) modes of the OH(4) group could be located at 1458 cm^{-1} and 1236 cm^{-1} respectively, indicating its existence in the enol form e.g., involving the amide function in positions 3, 4 [Scheme–(III – 1A)], in some amount. On coordination with the Mo – atom in different complexes (**3**, **4**, **5**), the above two IR bands disappear along with the appearance of a new band at around 1238 – 1275 cm^{-1} due to ν(C – O) mode of the corresponding phenoxide groups [Fig.(III – 11)] [85] involving deprotonation of OH(4).

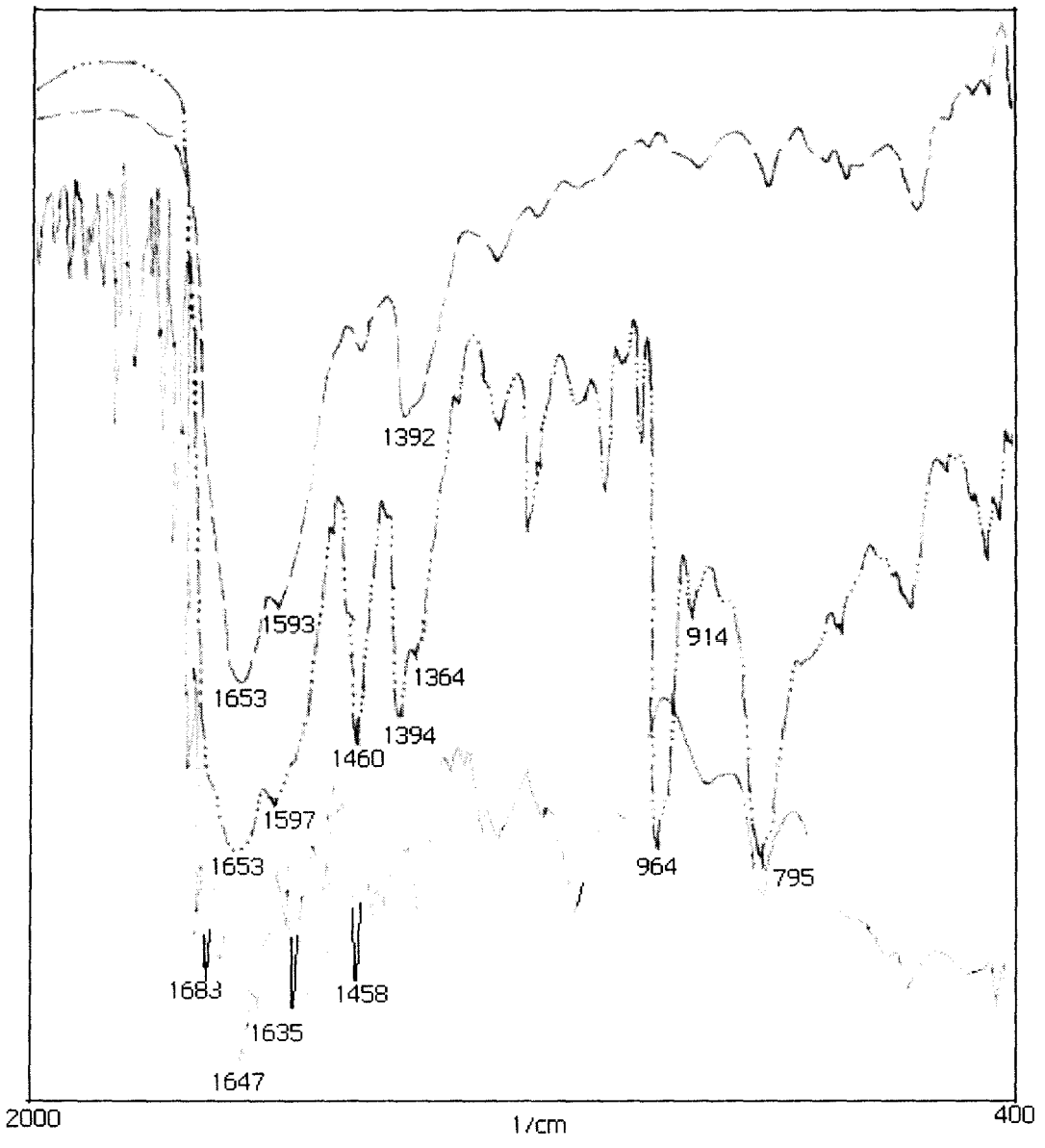

Fig.(III – 11): IR spectra (KBr) of (1)[——], (3) [— — —] and (4) [●●● —●●●]

Besides these, molecular modeling studies (CHEM3D, MM2 calculations corresponding to the lowest energy structure) as stated later indicate involvement of the S – atom (thiosemicarbazide residue) in the complexation process. The frequency of the IR band corresponding to ν(C=O) and ν(C=N) mode has increased from 1647 cm^{-1} in free ligand to 1653 cm^{-1} in the complexes [Fig.(III – 11)] corroborating the decrease in length of bond; such as C(3)-N(4) bond length has decreased from 1.3657 to1.3038 Å and C(19)-N(17) bond from 1.3730 to 1.2830 Å etc. which are presented in Table (III-8)

[atom numbering as per Fig.(III-12)]. Thus, it could be inferred that the Schiff base ligand (**1**) coordinates to the metal atom involving the three donor atoms e.g., O(4), N(5) and the S – atom. Usually tridentate bi-negative ligand coordination is observed except for one case where it is tri-negative.

As evident from Fig.(III – 11), some interesting inferences could be drawn regarding the presence or absence of oxomolybdenum core in these cases. In case of (**2**) there is no ν(Mo = O_t) or ν(Mo – O_b – Mo) band in the region 800 – 1000 cm^{-1} corresponding to its formulation here as devoid of any oxomolybdenum core. The same is true for complex (**3**). In complex (**4**) a pair of IR bands at 965 cm^{-1} [ν(Mo = O_t)] and another at 795 cm^{-1} [ν(Mo – O_b – Mo)] characteristic of $(Mo_2^{VI}O_3)^{6+}$ core could be identified [36]. This core has been identified structurally [55]. Appearance of these new bands in (**4**) verifies the oxygen atom transfer aspect of the conversion (**3**)→ (**4**) [Scheme-(III-3]. In compound (**5**) a new band appears at 790 cm^{-1} corresponding to the (Mo – O_b – Mo) mode. In (**6**) two new peaks characteristic of the $(Mo_2^{V}O_4)^{2+}$ core appear at 945 cm^{-1}, [ν(Mo = O_t)] and 790 cm^{-1}, [ν(Mo – O_b – Mo)] respectively. In (**7**) no IR band is observed in the region 800 – 1000 cm^{-1}, but a peak at 503 cm^{-1} [ν(Mo = S_t)] and another at 470 cm^{-1} [ν(Mo – S_b – Mo)] assignable to $(Mo_2^{VI}S_5)^{2+}$ core are observed [38].

^1H NMR data (DMSO-d_6) of (**1** – **7**) have been assigned on the basis of protonic integration data, multiplicity, ^1H–^1H COSY data and literature value [16(b), 85]. For (**1**) [Scheme (III – 1)] the – OH(4), NH(5) and NH(3) signals are observed at δ 12.49 (bs), δ 11.63 (bs), and δ 10.04 (bs) respectively indicating the presence of two tautomers [Scheme (III – 1A) and Scheme (III – 1B)] in DMSO solution. The NH_2 (γ), NH (β) and NH_2(2) signals are observed at δ 7.46 (bs), δ 7.30 (bs) and δ 7.11 (bs) respectively. Besides these, the $CH_2(1')$ and $CH_3(3')$ signals are observed at δ 3.57(d, br) and δ 2.22(t) respectively.

In the pertinent complexes (**2** – **7**) the –OH(4) signal is absent indicating its deprotonation. The NH(5) signal appears at downfield (δ 11.10 – 10.98, bs) as compared to the free ligand value in most cases indicating involvement of the NH(5) group in metal coordination process[3, 18, 20, 39]. Both the $CH_2(1')$ and $CH_3(3')$ signals are shielded in the

complexes and appear in the region δ 3.21 – 3.19 (q) and δ 1.20 – 1.18 (t) respectively. The NH_2 (γ) and NH_2(2) signals appear in the region δ 7.06 – 6.75 (bs) and δ 6.99 – 6.65 (bs) respectively, i.e., shielding is observed for these signals as well.

A comparison of the two Schemes [(III – 1) & (III - 2)] shows the basic change over in electronic structure of the Schiff base ligand (**1**) during the coordination process, as evident from IR and ^1H NMR spectral data, including attainment of aromatic character for the pyrimidine ring system of the pterin residue, it involves release of electron density through deprotonation of OH(4) and SH group. This imparts a reducing character to the ligand, leading to the reduction of the molybdenum (VI / V) starting materials during complex formation process. This change in electronic structure involving the entire ligand molecule is responsible for the above mentioned shielding process of the $CH_2(1')$, $CH_3(3')$, $NH_2(2)$ and NH_2 (γ) protons.

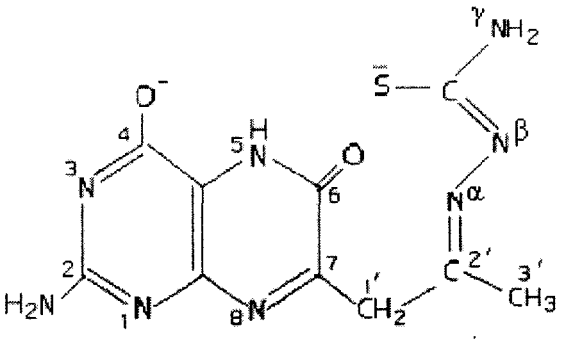

Scheme (III - 2)

The CH_3 – proton signal of CH_3OH and DMF in different complexes are partially buried under the residual solvent peak around δ 3.3 (absorbed water in DMSO-d_6); the proton signal of the H–C(=O)N< residue in DMF appears around δ 7.95. Although the –OH signal of CH_3OH appears around δ 5.0, in complexes (**2**) and (**7**) it appears at δ 12.34 (bs) indicating strong coordination of the – OH group of CH_3OH to the Mo – atom. Coordination of the CH_3OH molecule to the molybdenum atom in different types of compounds, sometimes leading to deprotonation / methoxide coordination, has been proposed by various workers and has been characterized by X-ray crystallographic data [3, 18, 20, 27].

Now the possible schematic structures of the new compounds were optimized by molecular mechanics calculation (MM2), giving the lowest steric energy (Kcal mol^{-1}) CHEM3D model [87] [e.g., Fig.(III –12) to Fig.(III – 18)], thereby throwing light on both stability and geometry of these compound. The molecular modelling force fields in use for molecular systems can be interpreted in terms of the four key contributions, e.g., bond stretching, angle bending, torsional terms and non-bonded interactions [86, 111, 112]; apart from the lowest steric energy of the molecule, two basic parameters were evaluated, e.g., bond distances (Å) and bond angles (deg.), the most relevant of which are shown in Table (III – 8) to Table (III – 14), together with the literature data obtained through X-ray structural studies on molybdenum complexes with different pterin ligands and other relevant compounds [3, 5, 20(a-c), 27, 29, 114, 115, 116]; this is in conformity with the recent trends of structure elucidation using optimized computational models [108, 113].

Concentrating on the chelating aspect of the pterin ligand towards molybdenum, the Mo-N(5) bond plays a pivotal role here [Scheme (III – 1) indicates the O(4), N(5) etc, numbering system] and their bond distances show a fair agreement between the computed and experimental data [3, 5, 20(a-c), 27, 29, 114, 115, 116]; the calculated Mo-O(4) bond distance is slightly shorter than the available X – ray structural data, but this value is close to the Mo – O_b bond distance (1.88 – 1.97 Å) of Mo – O_b – Mo bridges (of binuclear complex) and is much longer than the terminal Mo=O_t bond distance (1.66 – 1.67 Å)[3, 5, 20(a-c), 27, 29, 114, 115, 116].

Fig.(III –12) represents the most stable CHEM3D form (Steric energy = 10.006 Kcal mol^{-}) of (**1**). In this form, the pterin ligand contains the C(9)-substituent part (with the thiosemicarbazide residue) on the O(11), N(7)- side, as is present in the most stable CHEM3D representation of the metal complexes. The CHEM3D form which contains C(9)- substituent part on the N(6), N(10) side, possesses highest amount of energy among all the probable forms of (**1**) and not considered here.

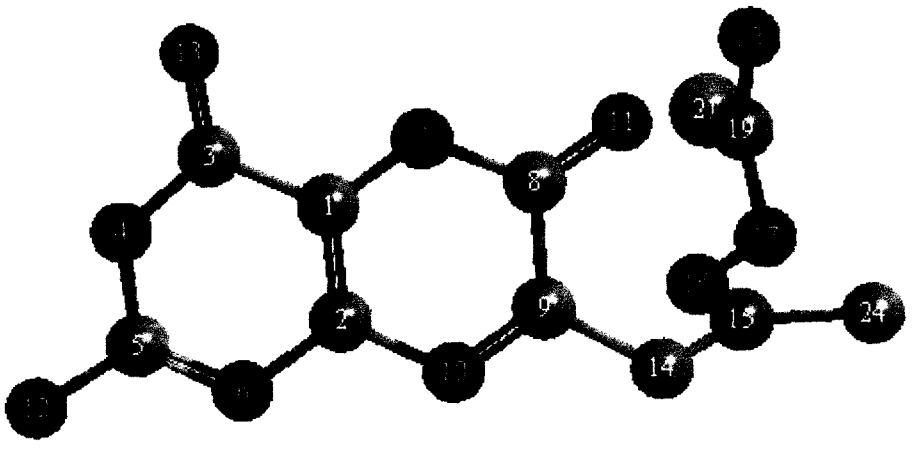

Fig.(III–12): The optimized geometry (CHEM3D model obtained through MM2 calculations) of (**1**) with a steric energy of 1.61 Kcal mol^{-1}. Its numbering system is set by the software used [87] and is different from that in Scheme (III – 1).

Table (III – 8): Comparison of selected optimized bond lengths (Å) and bond angles (deg.) in the free ligand (**1**) and its molybdenum complex (**2**)

Atoms	Bond Distances(Å)$^{+}$	Atoms	Bond Distances(Å)$^{+}$
C(1)-C(3)	1.47 [1.45]	C(19)-S(21)	1.58 [1.83]
C(1)-C(2)	1.37 [1.38]	N(4)-C(5)	1.35 [1.42]
C(1)-N(7)	1.35 [1.40]	C(5)-N(12)	1.37 [1.30]
C(9)-N(10)	1.28 [1.29]	C(3)-N(4)	1.36 [1.30]
C(19)-N(20)	1.37 [1.46]	C(9)-C(14)	1.50 [1.51]
C(14)-C(15)	1.50 [1.51]	C(2)-N(10)	1.41 [1.41]
C(8)-C(9)	1.49 [1.49]	C(19)-N(17)	1.37 [1.28]
C(15)-C(24)	1.49 [1.49]	C(5)-N(6)	1.31 [1.41]
N(16)-N(17)	1.36 [1.38]	C(15)-N(16)	1.26 [1.27]
C(3)-O(13)	1.23 [1.38]	N(7)-C(8)	1.36 [1.38]
C(8)-O(11)	1.22 [1.23]	C(2)-N(6)	1.41 [1.38]

Angle Atoms	Bond Angle(deg.)$^{+}$	Angle Atoms	Bond Angle(deg.)$^{+}$
N(10)-C(9)-C(8)	123.5 [122.9]	C(1)-C(3)-N(4)	114.9 [120.5]
C(9)-C(8)-N(7)	114.7 [114.9]	C(1)-C(2)-N(10)	120.5 [119.0]
C(5)-N(4)-C(3)	124.8 [117.6]	C(1)-C(2)-N(6)	121.3 [114.2]
N(4)-C(5)-N(6)	121.0 [121.5]	C(3)-C(1)-C(2)	118.4 [124.1]
C(9)-N(10)-C(2)	118.4 [118.8]	C(2)-C(1)-N(7)	120.5 [122.1]
C(1)-N(7)-C(8)	122.4 [118.1]	C(2)-N(6)-C(5)	119.6 [121.8]

$^{+}$From the respective optimized geometries (MM2 calculations) [87]. Atom numbering system corresponds to Fig.(III –12). Free ligand data are mentioned outside third bracket and the data derived from its molybdenum complex, (**2**), are mentioned within third bracket.

Tables (III – 8) shows the bond lengths and bond angles of the free ligand, $H_3(pte_2–tsc)$, and that of the pterin ligand residue in one of the complex of this series e.g., complex (**2**). Comparing these two sets of data it is clear that both bond lengths and bond angles of the ligand residue have undergone a visible change in it's complex suggesting definite complexation of the $H_3(pte_2–tsc)$ ligand with molybdenum metal. In comparison to the free ligand (**1**), the following bond lengths are increased in the complex: C(1) – N(7) from 1.35 Å to 1.40 Å, C(3) – O(13) from 1.23 Å to 1.38 Å and C(19) – S(21) from 1.58 Å to 1.83 Å. This observation is consistent with the N(7), O(13) and S(21) [Fig.(III –12)] atoms' bonding with the molybdenum atom [compare with Fig.(III –13)] leading to depletion of electron density from the bonds immediate to the bonds between the metal and these atoms (i.e., the bonds mentioned above) and hence the observed increase in bond lengths in the complex. The C(5) – N(12) bond length has undergone a decrease from 1.37 Å to 1.30 Å on complexation indicating the N(12) [N(2) as per Scheme – (III-1)] lone pairs' participation in metal coordination via the pterin rings. Some other bond lengths, such as, N(4) – C(5), C(19) – N(20), C(19) – N(17) etc. have also suffered visible change due to redistribution of overall electron density on metal coordination.

This observation is reflected in different physical data, such as, UV–VIS, ^{1}H NMR, fluorescence, IR spectra etc. of the free ligand (**1**) and its molybdenum complexes discussed later. All these data support increased electron density in the pterin rings of the ligand part in almost all the molybdenum complexes of (**1**).

Fig.(III –13) shows the lowest energy (Steric energy = 13.68 Kcal mol $^{-1}$) CHEM3D model of (**2**) containing slightly distorted trigonal bi-pyramidal (TBP) geometry around the Mo^{IV}-centre. The O(13), N(7) & S – atom of $[(pte_2\text{-}tsc)\}]^{3-}$ ligand residue occupy three coordination sites; and the methoxy group (CH_3O) and CH_3OH molecule complete the coordination geometry. The case of CH_3O- coordination is an X-ray crystallographically established one and reported by several authors [7(a),18(a)].

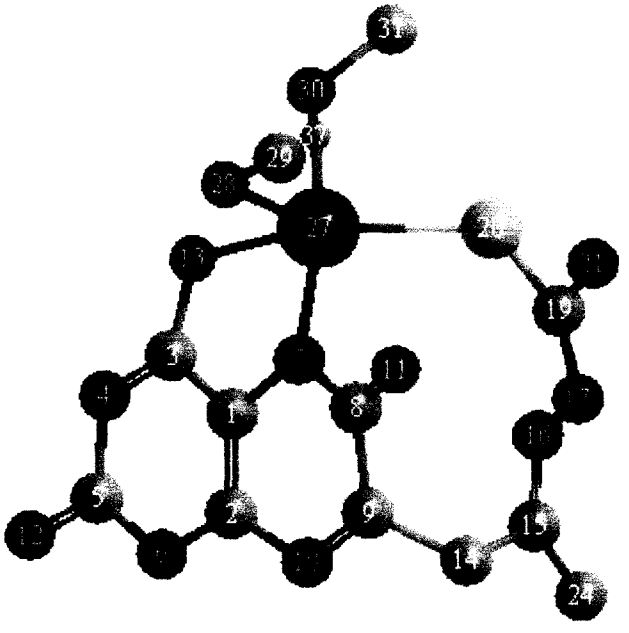

Fig.(III–13): **The optimized geometry (CHEM3D model obtained through MM2 calculations) of (2) with a steric energy of 13.68 Kcal mol $^{-1}$. Its numbering system is set by the software used[87] and is different from that in Schemes (III – 1).**

Table (III–9): Comparison of selected computed bond lengths(Å) and bond angles (deg.) involving Mo – atom in (**2**) from the optimized geometry [Fig.(III –13), MM2 calculations] with the available literature data (in parenthesis) from X-ray structural studies*

Atoms	Bond Distances(Å)+	Atoms	Bond Distances(Å)+
O(13)-Mo(27)	1.96(2.23)[3(c)]	O(30)-Mo(27)	2.07(2.32)[109]
S(20)-Mo(27)	2.33(2.37)[109, 110]	O(28)-Mo(27)	1.95
N(7)-Mo(27)	1.99(2.02)[3(c)]		

Angle Atoms	Bond Angle(deg.)+	Angle Atoms	Bond Angle(deg.)+
O(13)-Mo(27)-S(20)	153.9	S(20)-Mo(27)-N(7)	96.0
O(13)-Mo(27)-N(7)	81.4	O(28)-Mo(27)-N(7)	86.4
O(28)-Mo(27)-O(30)	87.6	O(13)-Mo(27)-O(30)	90.2
S(20)-Mo(27)-O(28)	126.8		

+ Here O(13) and N(7) correspond to O(4) and N(5) donor atoms respectively of the pterin ring as per Scheme (III – 1), while N(16), N(17) and N(21) correspond to N(α), N(β) and N(γ) respectively of the same scheme.

* X-ray structural data have been collected from the references mentioned as superscript on the data within parenthesis.

Table (III – 9) shows few relevant bond length and bond angle data of (**2**), together with the X-ray structural data on molybdenum complexes of pterin ligand obtained from the literature [3(c), 109, 110]. This approach of rationalizing optimized structural data, is in line with the recent trends in structure (and property) elucidation [48, 86, 108, 179]. The agreement between the computed bond lengths and the literature X-ray structural data is fair, especially for S(20) – Mo(27) and N(7) – Mo(27) [Table (III – 9)]. Of the different donor atoms from the pterin ligand, O(4) and N(5) atoms [this numbering system corresponds to Scheme (III – 1)] play a major role in the metal-ligand bonding process; incidentally in molybdenum–pterin complexes the pivotal role of the Mo-N(5) bond has been verified through X-ray crystallography [20(a,d), 27, 114, 115, 116]. From chemical and X-ray structural studies on 6-substituted pterins, it has been inferred that sufficiently

greater basicity / nucleophilicity resides at N(5) than at N(8) of the pterin ring, thereby influencing its above-mentioned coordinating ability [88(a), 119]. Another important factor in this direction is the close tally of Mo(27) – S(20) bond length from CHEM3D data with available X-ray data.. Considering the length of 7-sulpher chain [numbering as per Scheme (III – 1)] of the ligand, the S(20)-atom may be compared with that of a S – donor from peptide chain in oxomolybdoenzymes [2].

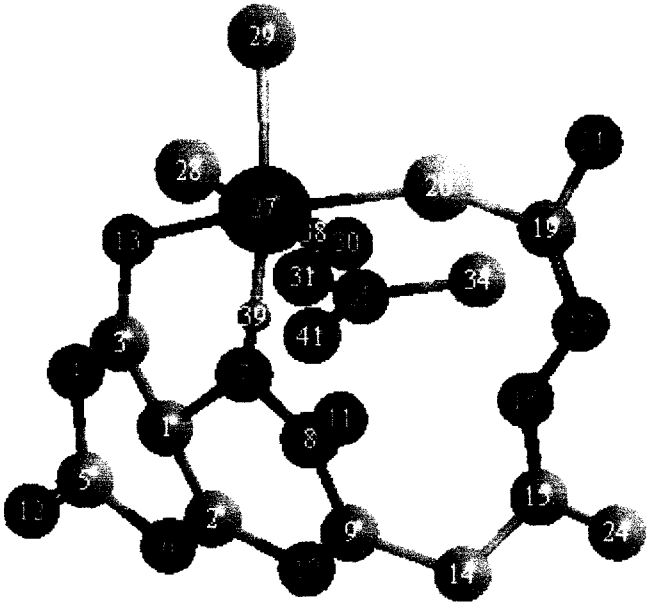

Fig.(III–14): The optimized geometry (CHEM3D model obtained through MM2 calculations) of (**3**) with a steric energy of 14.29 Kcal mol $^{-1}$. Its numbering system is set by the software used [87] and is different from that in Scheme (III– 1).

Table (III–10): Comparison of selected computed bond lengths(Å) and bond angles (deg.) involving the Mo – atom in (**3**) from the optimized geometry [Fig.(III –14), MM2 method] with the available literature data (in parenthesis) from X-ray structural studies*

Atoms	Bond Distances(Å)$^{+}$	Atoms	Bond Distances(Å)$^{+}$
S(20)-Mo(27)	2.34(2.37)[109,110]	Mo(27)-Cl(29)	2.31(2.38)[3(c)]
Cl(28)-Mo(27)	2.30(2.38)[3(c)]	N(7)-Mo(27)	2.14(2.02)[3(c)]
O(30)-Mo(27)	2.16(2.32)[109]	O(13)-Mo(27)	1.97(2.23)[3(c)]

Angle Atoms	Bond Angle(deg.)[+]	Angle Atoms	Bond Angle(deg.)[+]
S(20)-Mo(27)-Cl(29)	91.6	Cl(28)-Mo(27)-N(7)	88.8
Cl(28)-Mo(27)-O(30)	179.8	S(20)-Mo(27)-N(7)	96.7
Cl(28)-Mo(27)-O(13)	95.2	S(20)-Mo(27)-O(30)	89.5
N(7)-Mo(27)-O(30)	91.3	N(7)-Mo(27)-O(13)	80.2(74.1)[3(c)]
Cl(29)-Mo(27)-Cl(28)	93.7	O(30)-Mo(27)-O(13)	85.1
Cl(29)-Mo(27)-N(7)	171.4	C(3)-O(13)-Mo(27)	112.6(112.1)[3(c)]
Cl(29)-Mo(27)-O(30)	86.2	Mo(27)-N(7)-C(1)	117.5(119.3)[3(c)]
Cl(29)-Mo(27)-O(13)	91.3		

[+] Here O(13) and N(7) correspond to O(4) and N(5) donor atoms respectively, of the pterin ring as per Scheme (III – 1), while N(16), N(17)and N(21) correspond to N(α), N(β) and N(γ) respectively.

[*] X-ray structural data have been collected from references mentioned as superscript on the data within parenthesis.

The most stable (Steric energy = 14.29 Kcal mol $^{-1}$) CHEM3D representation of (**3**) shows a distorted octahedral geometry around the Mo^{IV}-atom [Fig.(III –14)]. The O(4), N(5) & S – atom of $[H(pte_2\text{-}tsc)\}]^{2-}$ ligand residue [Scheme(III–2)] have occupied three positions of the octahedron and other three positions are occupied by two Cl atoms and one DMF molecule. Here, N(5), and O- atom of the DMF molecule are bonded to the Mo –atom through co-ordinate bonds (pink colour) but the other four are covalent bonds.

Similar to the case of (**2**) above, there is a good matching between the computed and X-ray structural bond length and bond angle data of (**3**), especially for S(20)-Mo(27), N(7)-Mo(27), Mo(27)-Cl(28/29) [Table (III–10)]. This reflects the structural stability of (**3**) as presented in Fig.(III-14) above and supports the arguments / statements made for (**2**) in support of its correlation with oxomolybdoenzymes.

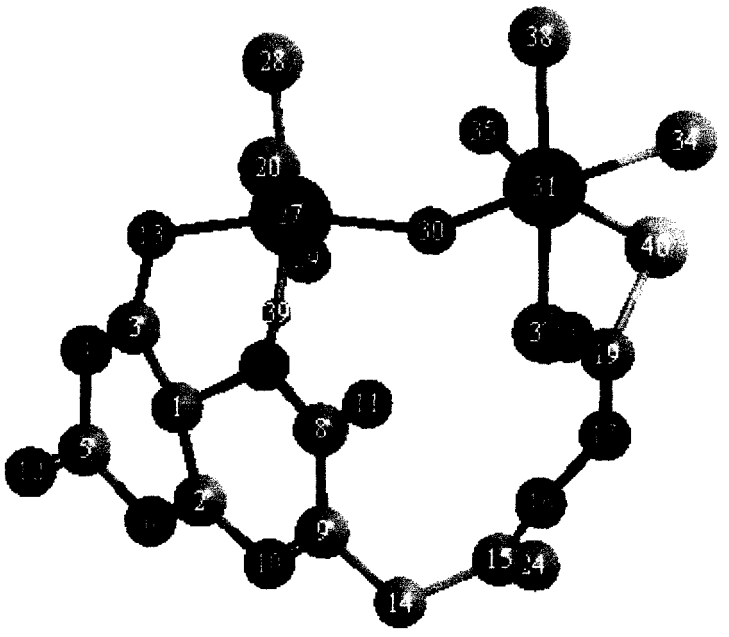

Fig.(III–15): The optimized geometry (CHEM3D model obtained through MM2 calculations) of **(4)** with a steric energy of 27.06 Kcal mol^{-1}. Its numbering system is set by the software used [87] and is different from that in Scheme (III – 1).

Table (III–11): Comparison of selected computed bond lengths(Å) and bond angles (deg.) involving the Mo – atom in **(4)** from the optimized geometry [Fig.(III–15), MM2 method] with the available literature data (in parenthesis) from X-ray structural studies*

Atoms	Bond Distances(Å)+	Atoms	Bond Distances(Å)+
S(40)-Mo(31)	2.35(2.37)[109, 110]	Mo(31)-Cl(34)	2.32(2.38)[3(c)]
N(7)-Mo(27)	2.16(2.02)[3(c)]	Mo(31)-Cl(38)	2.31(2.38)[3(c)]
Cl(28)-Mo(27)	2.31(2.38)[3(c)]	Mo(27)-Cl(20)	2.30(2.38)[3(c)]
Mo(31)-Cl(37)	2.31(2.38)[3(c)]	Mo(31)-O(35)	1.96(1.70)[108]
O(30)-Mo(31)	1.97(1.93)[19]	Mo(27)-O(29)	1.96(1.70)[108]
O(13)-Mo(27)	1.98(2.23)[3(c)]	Mo(27)-O(30)	1.97

Angle Atoms	Bond Angle(deg.)[+]	Angle Atoms	Bond Angle(deg.)[+]
Cl(38)-Mo(31)-O(30)	89.7(89.6)[108]	Cl(38)-Mo(31)-Cl(34)	90.0(91.9)[108]
N(7)-Mo(27)-O(13)	79.5(74.1)[3(c)]	C(3)-O(13)-Mo(27)	111.4(112.1)[3(c)]
C(1)-N(7)-Mo(27)	117.8(119.3)[3(c)]	O(29)-Mo(27)-O(13)	80.1
S(40)-Mo(31)-Cl(38)	91.6	O(30)-Mo(27)-N(7)	87.4
Cl(28)-Mo(27)-Cl(20)	95.0	Mo(27)-O(30)-Mo(31)	123.8
O(30)-Mo(27)-O(29)	96.2	O(35)-Mo(31)-O(30)	105.2
S(40)-Mo(31)-O(30)	89.4	O(30)-Mo(27)-O(13)	166.4
S(40)-Mo(31)-Cl(34)	86.1	Cl(28)-Mo(27)-O(13)	85.3
Cl(28)-Mo(27)-O(29)	86.0		

[+] Here O(13) and N(7) correspond to O(4) and N(5) donor atoms respectively, of the pterin ring as per Scheme (III – 1), while N(16), N(17)and N(21) correspond to N(α), N(β) and N(γ) respectively.

* X-ray structural data have been collected from references mentioned as superscript on the data within parenthesis.

Fig.(III –15) exhibits distorted octahedral geometry around each of the Mo^{VI} – atoms bonded through a bridging O- atom in its ($Mo^{VI}_2O_3$) core in the lowest energy (Steric energy = 27.06 Kcal mol^{-1}) structural form of (**4**). The O(4) & N(5) of [H(pte_2-tsc)}]$^{2-}$ ligand residue [Scheme (III – 2)] make covalent and co-ordinate (pink colour) bonds respectively to one of the two Mo-atoms. The S – atom of the C(7)-substituent is coordinated to another molybdenum atom. All the other bonds to the metal atoms are covalent in nature. Two (Mo = O_t) bands of the ($Mo^{VI}_2O_3$) core are essentially cis in nature here, as revealed from different bond angles data in Table (III–11). Actually X-ray structural data on different pteridine system indicate non-planarity corresponding to the most stable thermodynamic form [88].

The close tally of Mo(31)–S(40) bond length from CHEM3D data with available X-ray data is significant. Considering the length of 7-sulpher chain [numbering as per Scheme (III – 1)] of the ligand, the S(40)-atom may be compared with that of a S–donor from peptide chain in oxomolybdoenzymes [2]. The close agreements in other cases namely, N(7)-Mo(27), Mo(27/31)-Cl(20/28/34/37/38) etc. bond lengths and Cl(38)-Mo(31)-O(30), Cl(38)-Mo(31)-Cl(34), C(3)-O(13)-Mo(27), C(1)-N(7)-Mo(27) etc. bond angles supports the CHEM3D data discussions already made above in case of **(2)**.

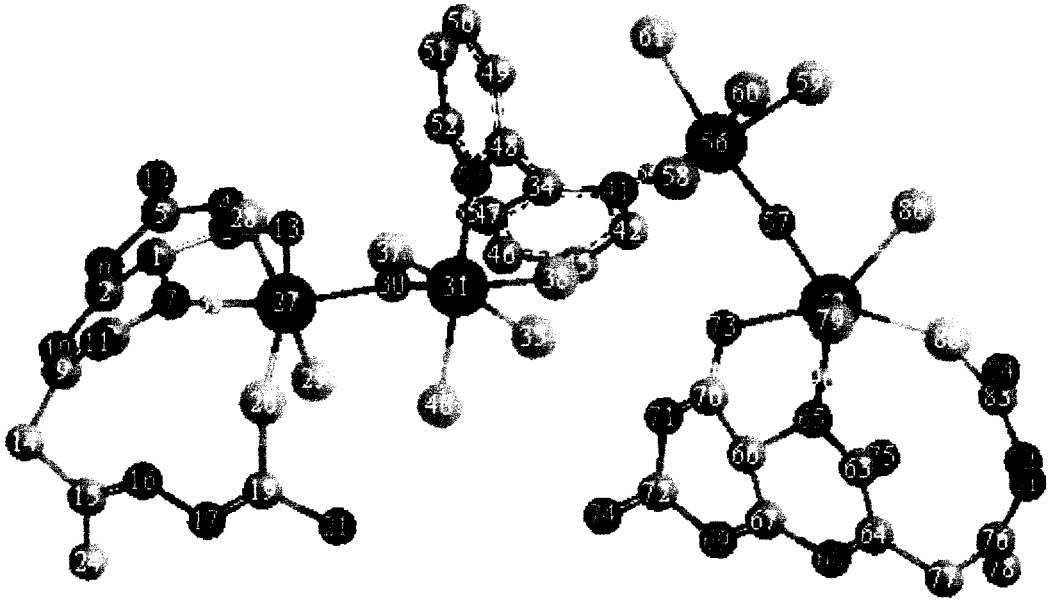

Fig.(III–16): The optimized geometry (CHEM3D model obtained through MM2 calculations) of **(5)** with a steric energy of 57.23 Kcal mol^{-1}. Its numbering system is set by the software used [87] and is different from that in Scheme (III – 1).

Table (III–12): Comparison of selected computed bond lengths(Å) and bond angles (deg.) involving the Mo – atom in **(5)** from the optimized geometry [Fig.(III –16), MM2 method] with the available literature data (in parenthesis) from X-ray structural studies*

Atoms	Bond Distances(Å)+	Atoms	Bond Distances(Å)+
N(41)-Mo(56)	2.13(2.02)[3(c)]	Mo(27)-Cl(29)	2.31(2.30)[3(c)]
S(20)-Mo(27)	2.34(2.37)[109, 110]	N(53)-Mo(31)	2.12(2.18)[109]
N(7)-Mo(27)	2.17(2.02)[3(c)]	Mo(31)-Cl(40)	2.32(2.30)[3(c)]

Mo(56)-Cl(58)	2.31(2.30)[3(c)]	O(73)-Mo(62)	2.00(2.229)[3(c)]
Mo(56)-Cl(60)	2.32(2.30)[3(c)]	Mo(31)-Cl(38)	2.32(2.30)[3(c)]
O(30)-Mo(31)	1.98(2.30)[3(c)]	S(86)-Mo(62)	2.37(2.37)[109, 110]
Mo(56)-Cl(61)	2.32(2.30)[3(c)]	O(13)-Mo(27)	1.98(2.23)[3(c)]
N(65)-Mo(62)	2.24(2.02)[3(c)]	Mo(62)-Cl(80)	2.34(2.30)[3(c)]
Mo(31)-Cl(35)	2.31(2.30)[3(c)]	Mo(27)-O(30)	1.97(1.93)[19]

Angle Atoms	**Bond Angle(deg.)**[+]	**Angle Atoms**	**Bond Angle(deg.)**[+]
N(65)-Mo(62)-O(73)	74.1(74.1)[3(c)]	Cl(38)-Mo(31)-Cl(35)	90.8(91.1)[108]
C(3)-O(13)-Mo(27)	114.7(112.1)[3(c)]	C(1)-N(7)-Mo(27)	118.02(119.3)[3(c)]
N(53)-Mo(31)-Cl(40)	179.8	O(57)-Mo(62)-O(73)	76.0
Cl(37)-Mo(31)-Cl(40)	86.6	Cl(37)-Mo(31)-Cl(38)	82.7
Cl(37)-Mo(31)-Cl(35)	169.3	N(7)-Mo(27)-S(20)	87.9
N(65)-Mo(62)-S(86)	74.5	O(30)-Mo(31)-Cl(38)	165.6
O(30)-Mo(31)-Cl(35)	78.8	Cl(40)-Mo(31)-Cl(38)	88.6
O(73)-Mo(62)-S(86)	148.1	Mo(31)-O(30)-Mo(27)	126.7
N(7)-Mo(27)-O(13)	81.0	N(53)-Mo(31)-Cl(37)	93.6
N(7)-Mo(27)-O(30)	164.1	S(20)-Mo(27)-O(30)	107.7
N(41)-Mo(56)-O(57)	91.1	S(20)-Mo(27)-O(13)	167.6

[+] Here O(13/73) and N(7/65) correspond to O(4) and N(5) donor atoms respectively, of the pterin ring as per Scheme (III – 1), while N(16/81), N(17/82)and N(21/84) correspond to N(α), N(β) and N(γ) respectively.

* X-ray structural data have been collected from references mentioned as superscript on the data within parenthesis.

Fig.(III –12) represents the lowest energy (Steric energy = 57.23 Kcal mol $^{-1}$) CHEM3D model geometry of (**5**). Here, again the aromatic or planner nature of the pterin ligand residue hinders its needed puckering in this bulcky molecule and lowers its stability. The geometry around each Mo^{V} – atom is distorted octahedral. Here, O(4) & S – atom of $[H(pte_2\text{-}tsc)\}]^{2-}$ ligand residue [Scheme (III – 2)] and all the Cl – atoms make covalent bonds with the metal atoms, while N(5) of pterin ring and the N – atoms of 'bipy' are bonded to the Mo^{V} – atom through co-ordinate bonds (pink colour). Air stability (low hygroscopic nature) of this tetra-nuclear species indicates that the Mo^{V} – atoms are saturated with respect to both electronegativity as well as co-ordination number. Interesting aspect of synthesis of this compound is that the original starting material, $[Mo^{V}OCl_3(bipy)]$, contained 3Cl atoms per Mo atom and the product (**5**), also maintains the same ratio, Mo : Cl = 1 : 3. Some of the 'bipy' ligands are lost and the vacant co-ordination positions are taken up by the $[H(pte_2\text{-}tsc)\}]^{2-}$ ligand residue as well as by the bridging O – atoms.

The ESIMS peak of (**5**) at m/z = 894.3, $[M/2 - Cl - 3H]^{+}$, can also be interpreted in the light of CHEM3D optimized geometry of the complex [Fig.(III –16)]. Origination of this peak corresponds to the breakage of the actual tetra-nuclear molecule into two binuclear species, followed by loss of one chlorine and three hydrogen atoms from each, where 'M' is the molecular formula of the complex (F.W.=1865.76.)[7(a), 14, 15]. This symmetric cleavage is possible by breaking of C(34) – C(48) bond of the bipyridyl residue in the molecular structure of (**5**).

Some specific data such as, Mo(27/62)– S(20/86), Mo(27/31/56/62)– N(7/53/41/65) etc. bond lengths and N(65)-Mo(62)-O(73), Cl(38)-Mo(31)-Cl(35) etc bond angles show close tally with the X-ray structural data and this is consistent with the above CHEM3D data interpretation for (**2**).

The lowest energy CHEM3D model geometry (Steric energy = 58.49 Kcal mol $^{-1}$) of (**6**) is represented in Fig.(III–17). It has a distorted octahedral geometry around both the Mo^{V} – atoms, O(4) & S –atom of $[H(pte_2\text{-}tsc)\}]^{-2}$ ligand residue [numbering system as per Scheme (III – 2)] are bonded to the Mo – atoms through covalent bonds, whereas, N(5) and O –atoms from the DMF molecules are bonded to the metal atom via the formation of co-ordinate bond (pink colour). Pterin ring's O(4) & N(5) – atoms are bonded to one Mo – atom and the C(7)-substituent's S – atom along with two DMSO molecules are bonded to another Mo – atom of the $(Mo^{V}_2O_4)^{2+}$ core. From the bond angle data [Table (III-13)] of O(37)-Mo(27)-O(28) (= 77.7630) and O(30)-Mo(31)-O(35) (= 72.5074) involving the two terminal oxygen atoms, it can be inferred that the $(Mo^{V}_2O_4)^{2+}$ core in (**6**) is essentially trans in nature [Fig.(III–17)]. Its cis isomer was found to be comparatively less stable.

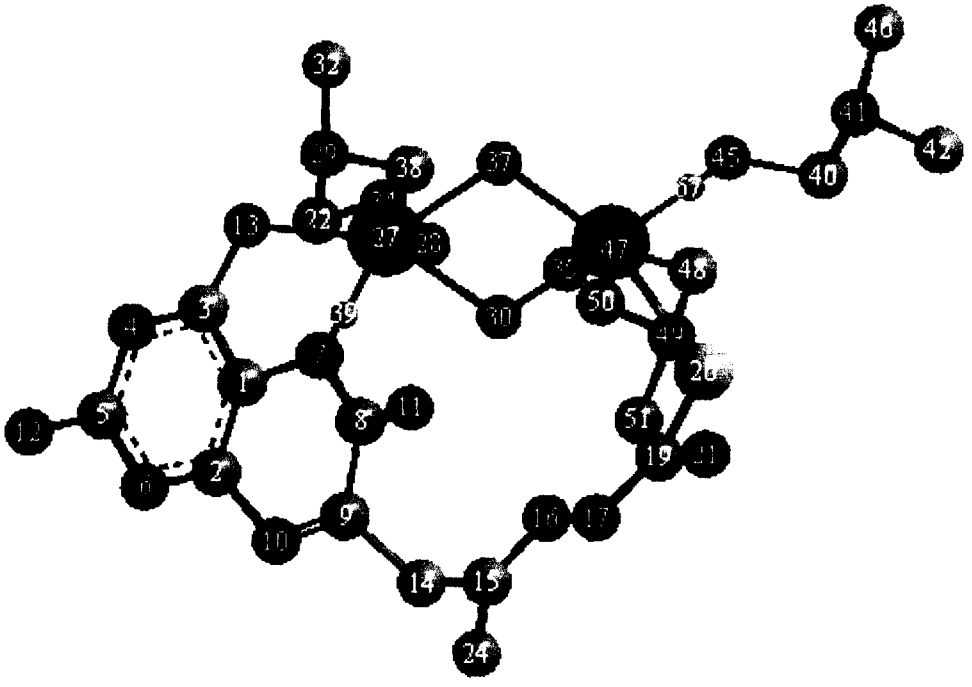

Fig.(III–17): The optimized geometry (CHEM3D model obtained through MM2 calculations) of (**6**) with a steric energy of 58.49 Kcal mol $^{-1}$. Its numbering system is set by the software used [87] and is different from that in Scheme (III – 1).

Table (III–13): Comparison of selected computed bond lengths(Å) and bond angles (deg.) involving the Mo–atom in (**6**) from the optimized geometry [Fig.(III–17), MM2 method] with the available literature data (in parenthesis) from X-ray structural studies*

Atoms	Bond Distances(Å)+	Atoms	Bond Distances(Å)+
S(20)-Mo(31)	2.33(2.37)[109, 110]	N(7)-Mo(27)	2.16(2.02)[3(c)]
O(34)-Mo(27)	2.09(2.01)[109]	O(47)-Mo(31)	2.11(2.01)[109]
O(13)-Mo(27)	2.02(2.23)[3(c)]	O(28)-Mo(27)	1.94(1.70)[109]
Mo(31)-O(35)	1.96(1.70)[109]	O(30)-Mo(31)	1.97(1.93)[19]
Mo(27)-O(30)	2.01		

Angle Atoms	Bond Angle(deg.)+	Angle Atoms	Bond Angle(deg.)+
N(7)-Mo(27)-O(13)	74.4(74.1)[3(c)]	Mo(27)-O(13)-C(3)	111.5(112.1)[3(c)]
Mo(27)-N(7)-C(1)	114.6(119.3)[3(c)]	O(45)-Mo(31)-O(35)	107.0(105.9)[109]
S(20)-Mo(31)-O(37)	160.2(153.0)[109]	S(20)-Mo(31)-O(35)	93.8(97.7)[109]
O(37)-Mo(27)-O(28)	77.8	O(30)-Mo(31)-S(20)	90.2
O(30)-Mo(31)-O(35)	72.5	O(37)-Mo(27)-O(30)	69.4
O(47)-Mo(31)-O(37)	91.2		

+ Here O(13) and N(7) correspond to O(4) and N(5) donor atoms respectively, of the pterin ring as per Scheme (III – 1), while N(16), N(17)and N(21) correspond to N(α), N(β) and N(γ) respectively.

* X-ray structural data have been collected from references mentioned as superscript on the data within parenthesis.

Almost all the bond lengths especially S(20)-Mo(31), O(34)-Mo(27), O(47)-Mo(31), N(7)-Mo(27) etc., show good matching between the computed and single crystal X-ray structural data supporting the interpretation presented above for (**2**) regarding bond length / bond angle data.

Fig.(III–18) reflects slightly distorted octahedral geometry of the new complex (7), in the lowest energy form (Steric energy = 29.22 Kcal mol $^{-1}$), in which the Mo^{VI} – centers have slightly distorted octahedral geometry. Here, the ligand residue, $[H(pte_2\text{-}tsc)\}]^{2-}$, acts as a binegative O(4), N(5), S – donor [numbering system as per Scheme (III-2)], in which the O(4) & S – atoms co-ordinated by covalent bond formation and N(5) & methanolic O – atoms are bonded to the Mo – centers through co-ordinate bond formation (pink colour). Here, $(Mo^{VI}_2S_5)^{2+}$ core is essentially in trans form, as supported by the magnitude of S(28)-Mo(31)-S(30) and S(32)-Mo(27)-S(30) bond angles [Table (III–14)]. The unique nature of $(Mo^{VI}_2S_5)^{2+}$ core is verified through elemental analysis, ESIMS data and CHEM3D optimized structural matching with the available X-ray structural data. This optimized geometry contains non – aromatic pterin ligand residue which gave the most stable, lowest energy form.

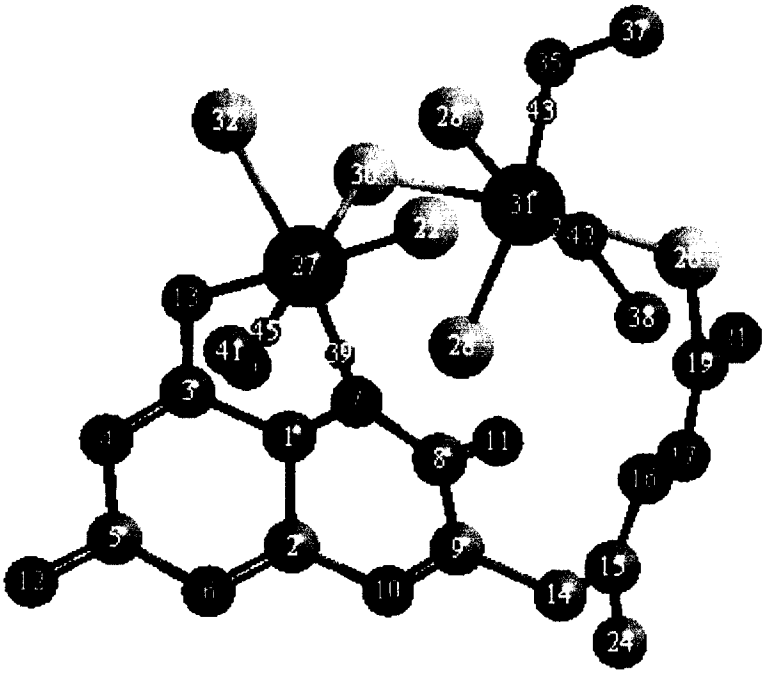

Fig.(III–18): The optimized geometry (CHEM3D model obtained through MM2 calculations) of (7) with a steric energy of 29.22 Kcal mol $^{-1}$.Its numbering system is set by the software used [87] and is different from that in Scheme (III – 1).

Table (III–14): Comparison of selected computed bond lengths(Å) and bond angles (deg.) involving the Mo – atom in (**7**) from the optimized geometry [Fig.(III –18), MM2 method] with the available literature data (in parenthesis) from X-ray structural studies*

Atoms	Bond Distances(Å)+	Atoms	Bond Distances(Å)+
S(20)-Mo(31)	2.34(2.37)[109, 110]	N(7)-Mo(27)	2.15(2.02)[3(c)]
O(13)-Mo(27)	1.97(2.23)[3(c)]	O(42)-Mo(31)	2.10 (2.32)[109]
O(40)-Mo(27)	2.08(2.32)[109]	Mo(27)-S(22)	2.34
S(30)-Mo(31)	2.35(2.30)[19]	Mo(31)-S(28)	2.35
Angle Atoms	**Bond Angle(deg.)+**	**Angle Atoms**	**Bond Angle(deg.)+**
Mo(27)-O(13)-C(3)	114.7(112.1)[3(c)]	C(1)-N(7)-Mo(27)	116.0(119.3)[3(c)]
N(7)-Mo(27)-O(13)	81.5(74.1)[3(c)]	O(42)-Mo(31)-S(28)	162.8(153.0)[109]
O(40)-Mo(27)-N(7)	81.7	S(28)-Mo(31)-S(20)	87.8
O(40)-Mo(27)-O(13)	88.4	O(40)-Mo(27)-S(32)	99.2
S(28)-Mo(31)-S(30)	91.4	S(32)-Mo(27)-S(30)	86.4
O(13)-Mo(27)-S(30)	86.3	Mo(31)-S(20)-C(19)	117.7
Mo(31)-S(30)-Mo(27)	122.6	O(40)-Mo(27)-S(22)	85.4

+ Here O(13) and N(7) correspond to O(4) and N(5) donor atoms respectively, of the pterin ring as per Scheme (III–1), while N(16), N(17)and N(21) correspond to N(α), N(β) and N(γ) respectively.

* X-ray structural data have been collected from references mentioned as superscript on the data within parenthesis.

Similar to the cases of other compounds discussed above, almost all the computed bond lengths and bond angles show good agreement with the available single crystal X-ray data. Some noteworthy cases are, S(20)-Mo(31), N(7)-Mo(27) etc., bond lengths which corroborate the arguments / statements made above regarding CHEM3D data interpretation of (**2**).

The above discussion on the geometrical aspect of optimized computational model (MM2) of the new complex compounds, having agreement with available X-ray structural data (e.g., bond length, bond angle and overall geometry) provides the frame work for discussion on their spectroscopic, reactivity and other relevant aspects [108, 113]. All the molybdenum complexes discussed in this Chapter, show essentially four types of computed bond angles (70 ° – 86 °, 88° – 100 °, 105 ° – 130 ° and 138 ° – 179 °), which are in complete agreement with the X-ray structural studies on different molybdenum – pterin systems with the respective geometries around the Mo – atoms (both mono and binuclear types) [3, 5, 20(a-c), 27, 114, 115, 116].

Some important observations are made from the comparative study of UV-VIS absorption spectroscopy of the ligand (**1**) and that of its molybdenum complexes. Three bands of (**1**) at 310 nm, 355.5 nm and 408 nm are completely modified in the metal complexes and appear at lower wave lengths and with larger intensity, except in (**6**), where 408 nm ligand peak is missing. A sharp increase in intensity of the UV-VIS absorption bands in the metal complexes can be accounted for [34] electronic drift from – $NH_2(2)$ group [Scheme (III–2)] towards metal – ligand bonding site via the pterin ring enhancing electron density (essentially π) in the ligand part and hence the increased intensity in the absorption bands of (**2**) to (**7**) [3, 20(a)]. The phenomenon of $NH_2(2)$ lone pair's participate in metal coordination via the pterin rings is verified by the shortening of N(2)-C(2) [Scheme (III-2)] bond length on coordination with molybdenum atom, as discussed above regarding the interpretation of CHEM3D optimized geometry data of compounds (**2**) to (**7**). That metal – pterin coordination leads to greater electron flow resulting higher electron density around the coordination site and other parts of the molecule, are also substantiated by ^1H NMR and fluorescence study [Fig.(III–28)].

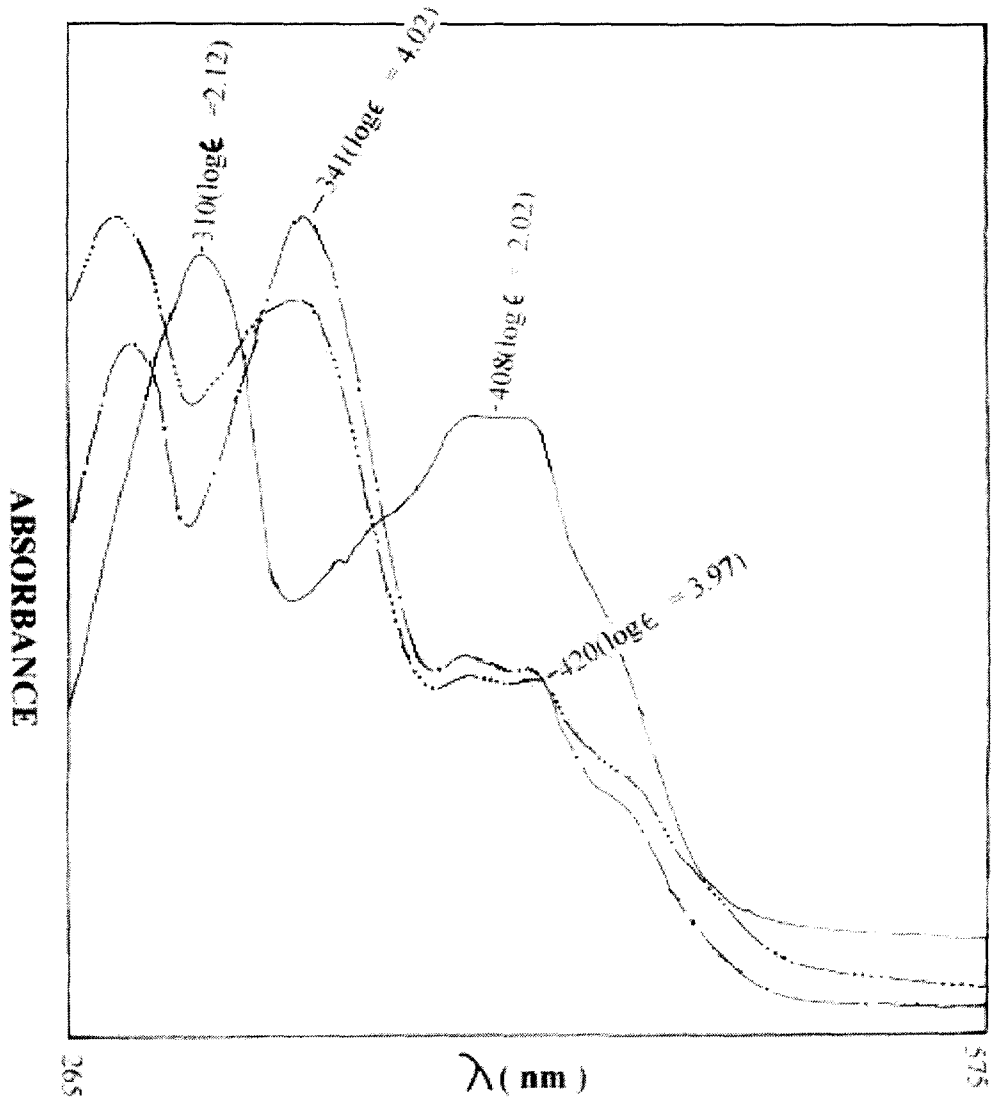

Fig.(III-19) : UV-VIS absorption spectra of (**1**) [——], (**2**) [– · – · –] and (**7**) [– · · · · –] in DMF.

Another interesting phenomenon observed is the appearance of UV-VIS absorption bands at wave–lengths higher than 400 nm in these complexes [Fig.(III–19)]. One such band is observed at about 420 nm and another at 453 nm. These bands are essentially metal to ligand charge transfer (CT) bands [8(a,b)] ; which are absent in the case of the ligand (**1**). Another high wave length CT band is observed at 491 nm (3.84) in case of (**5**) and at 486 nm (3.49) for (**6**).

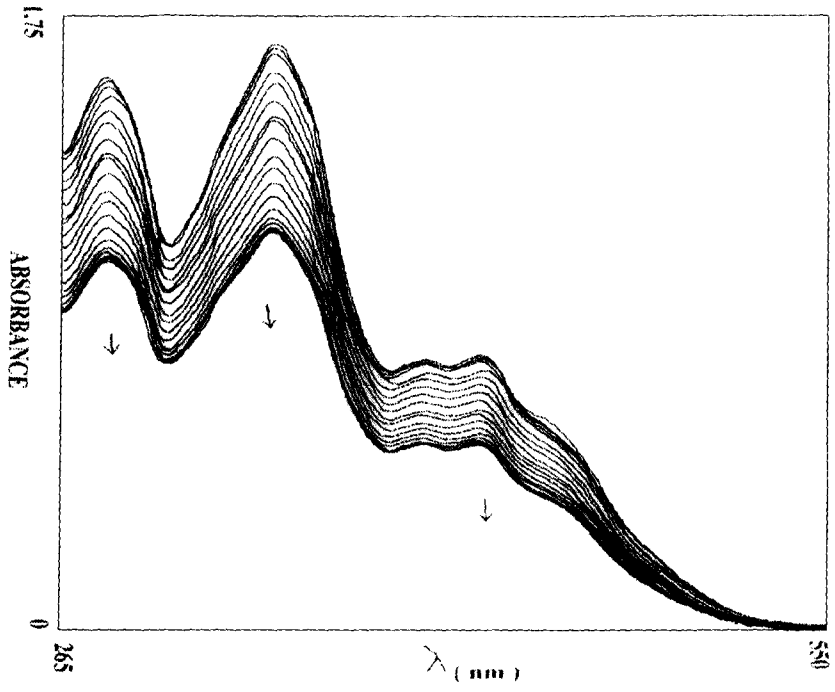

Fig.(III–20): UV–VIS absorption spectral changes recorded every 15 min. during the reaction of (**2**) [$1.0x10^{-4}$(M)] with PyN→O [$1.7x10^{-3}$(M)] in DMF at 301K.

All the present complexes (**2–7**) proved to be susceptible to oxygen atom transfer (OAT) reactions, along with coupled electron proton transfer (CEPT) reactions in some cases. Compounds (**2**), (**3**), (**5**) & (**6**) having metal centre (Mo – atom) in lower oxidation states (IV or V) show reactivity with potent oxygen donor species (typical enzyme substrate), like pyridine N – oxide (PyN→O), trimethyl amine N–oxide (Me_3N→O) [Fig.s (III–20), (III–22), (III–26) & (III–29)], whereas, they do not react with oxygen abstractor, e.g., triphenyl phosphine (PPh_3). The oxygen donor species, oxidize compounds (**2**), (**3**), (**5**) & (**6**) to some higher oxidation state and itself getting reduced to pyridine (PyN) or trimethyl amine (Me_3N). This indicates that these complexes are in the reduced state. Spectrophotometric study of these reactions in an overlay mode

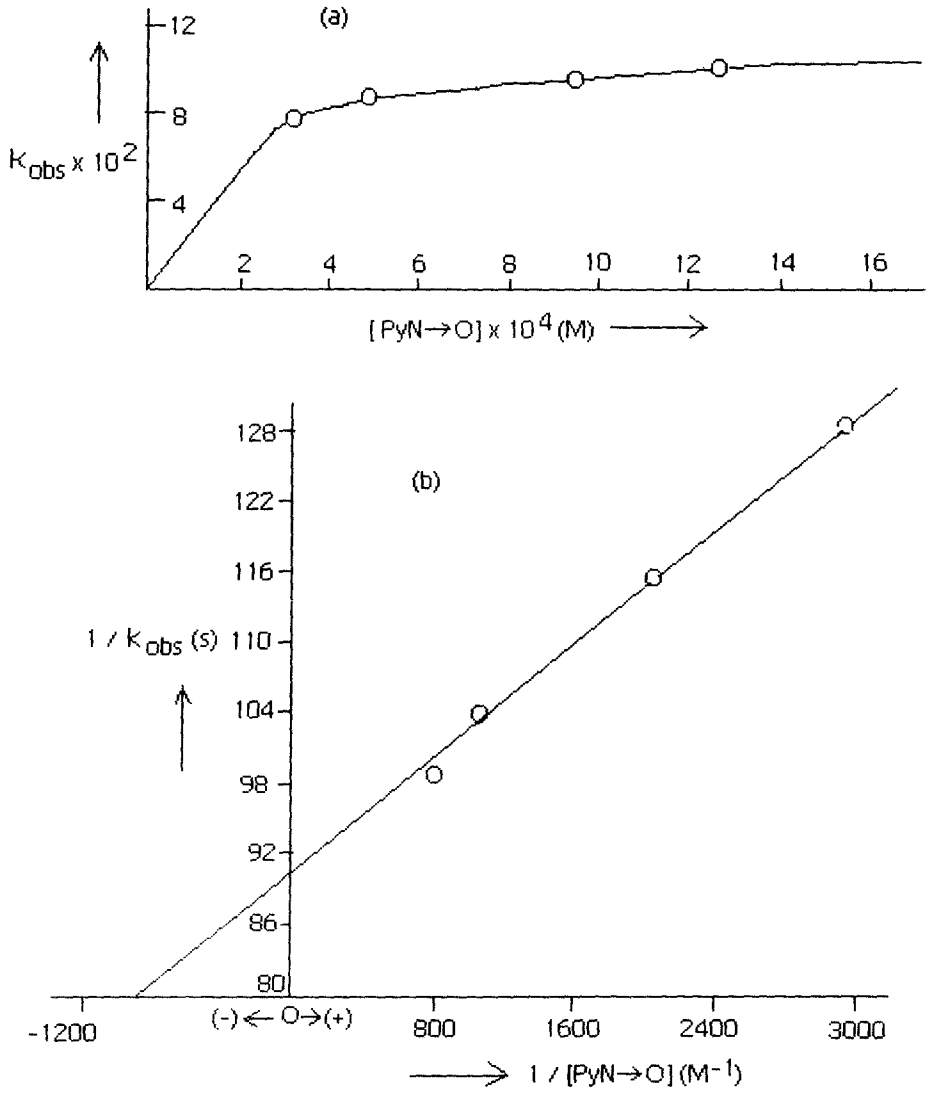

Fig.(III–21): (a)Dependence of the rate of reaction of (**2**) [2.9x10 $^{-5}$(M)] with PyN→O in DMF at 301 K; (b) the corresponding double reciprocal plot.

clearly shows UV-VIS absorption change in the metal – centred charge transfer region as well as intra ligand transition [Fig.s (III–20), (III–22), (III–26) & (III–29) respectively]. So, it is the Mo-atom in these complexes which is the site of oxygen atom transfer reaction.

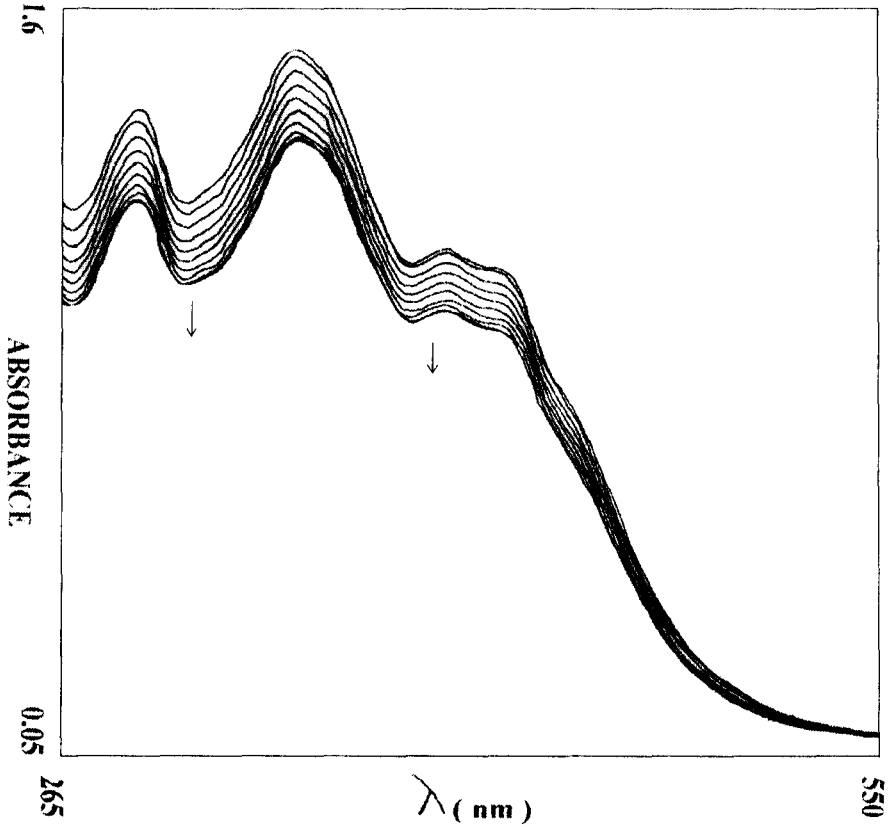

Fig.(III – 22): UV–VIS absorption spectral changes recorded every 13 min. during the reaction of (**3**) [$6.76x10^{-5}$(M)] with $Me_3N \rightarrow O$ [$2.2x10^{-3}$(M)] in DMF at 301K.

But these molybdenum – pterin complexes have been synthesized from molybdenum starting materials (having V or VI metal oxidation states) and are reduced [except (**5**)] to some lower oxidation state (Mo^{V} or Mo^{IV}) during their synthesis. So, the ligand here acts as a reducing agent. In case of (**5**), as the starting material was already in reduced state (Mo^{V}), probably for this reason it did not undergo any further reduction by the ligand. Compounds (**4**) & (**7**) undergo reaction with a typical oxygen abstractor like PPh_3 and UV-VIS spectrophotometric monitoring of such reactions have been recorded [Fig.s (III–24) & (III–32) respectively]. This indicates that the Mo – atoms in these compounds are in the higher oxidation state(e.g.,VI). This further corroborates the presence of oxomolybdenum and thiomolybdenum core in (**4**) & (**7**) respectively, as shown in their molecular formulas[36] and established by elemental analysis and ESIMS

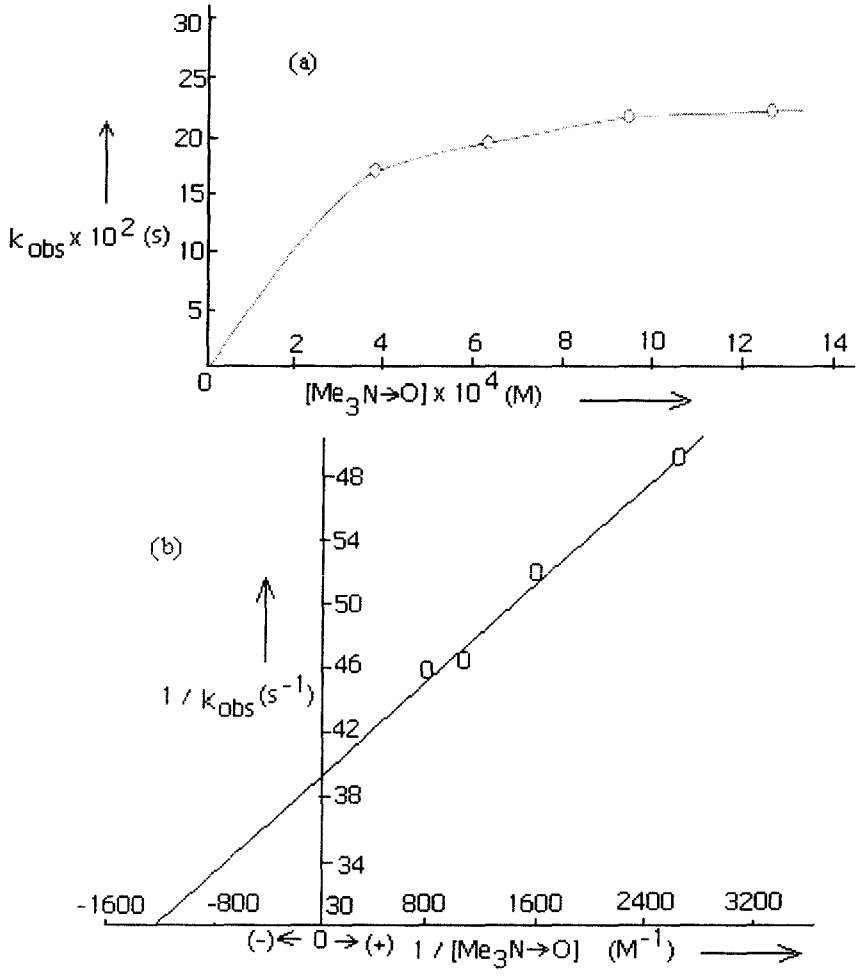

Fig.(III–23):(a)Dependence of the rate of reaction of (**3**) [3.46x10 $^{-5}$(M)] with $Me_3N \rightarrow O$ in DMF at 301 K; (b) the corresponding double reciprocal plot.

data. In case of (**4**) , existence of Mo^{VI} – centre is likely as it was prepared from (**3**) (a Mo^{IV} compound) by prolong aerial oxidation. Exceptional nature of (**7**) with a Mo^{VI} – centre (i.e., the Mo – centre not undergoing reduction during complex synthesis), can be correlated with oxidizing property of the $(MoS_4)^{2-}$ starting material; formation of $(Mo^{VI}_2S_5)^{2-}$ core is also in line with the unique behavior of the Mo – S duo [41] in nature as well as in synthetic system.

Oxidation / reduction of these complexes by $Me_3N \rightarrow O$, $PyN \rightarrow O$ / PPh_3 is also substantiated through fluorescence study of these molybdenum – pterin complexes and of their oxidized / reduced products. The oxidized product shows ca. one–third fluorescence intensity than that for the original complex [Fig.(III – 28)(a)]. Similarly, the reduced product has 2 – 3 times more intensity in its fluorescence spectrum compared to that of the original complex [Fig.(III – 28(b)]. This observation can be correlated with the electronic structure of the complexes on the basis of higher electron density generated in the complex due to its reduction by PPh_3 and similarly decrease of electron density after oxidation by $Me_3N \rightarrow O$ / $PyN \rightarrow O$. Hence, fluorescence spectral study can be a valuable probe for studying the changes in electronic structure during their reaction.

In few cases, quantitative aspects of these oxygen atom transfer reactions have been established by studying reaction stoichiometry for assigning oxidation state of the metal centers. A known weight of (**2**) was reacted with its ten equivalent of $PyN \rightarrow O$ in DMF (100 ml) (328K, 50h, N_2- atm., darkness) and the amount of pyridine released was estimated gravimetrically as the known compound $[Zn(C_5H_5N)_2](SCN)_2$ from the petroleum ether extract of the reaction medium[25]. About two moles of pyridine was recovered per mole of (**2**) added as per the following equations [1(a) and 1(b) are different steps leading to overall reaction (1)]:

$$2 \text{ x compound } (\mathbf{2}) + 2PyN \rightarrow O \longrightarrow 2\,[Mo^{VI}O]^{4+} \text{ complex} + 2PyN \text{ --1(a)}$$

$$2\,[Mo^{VI}O]^{4+} \text{ complex} + 2PyN \rightarrow O + H_2O \longrightarrow [Mo_2{}^{VI}O_5]^{2+} \text{complex} + 2PyN + 2H^+ \text{ --- 1(b)}$$

The overall reaction :

$$2 \text{ x compound } (\mathbf{2}) + 4PyN \rightarrow O + H_2O \longrightarrow [Mo_2{}^{VI}O_5]^{2+} \text{complex} + 4PyN + 2H^+ \text{ --- (1)}$$

The relevant oxidation product was isolated by evaporation in rotary evaporator, followed by treatment of the residue with methanol, filtration and washing with ether. Physico-chemical studies indicate the composition $[(Mo^{VI}_2O_5)\{H(pte\text{-}tsc)\}(DMF)_3]$. The ν(Mo = O) and ν(Mo – O – Mo) modes characteristic of the $[Mo_2^{VI}O_5]^{2+}$ core are observed at 925 cm^{-1}, 888 cm^{-1} and 825 cm^{-1} respectively [20]. H_2O used in Equation 1(b), most probably came from moisture in the solvent and took part in the hydrolysis of $[Mo^{VI}O]^{4+}$ core followed by oxo – dimerization to give $[Mo_2^{VI}O_5]^{2+}$ species (Equation 1)[19, 20(c,d)].

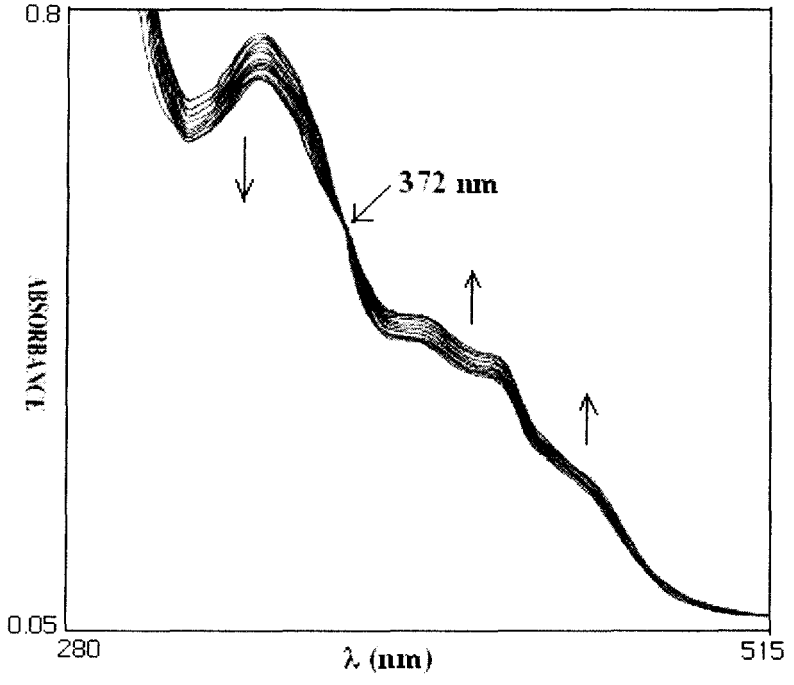

Fig.(III–24): UV–VIS absorption spectral changes recorded every 20 min. during the reaction of (**4**) [$3.5x10^{-5}$(M)] with PPh_3 [$2.86x10^{-4}$(M)] in DMF at 301K.

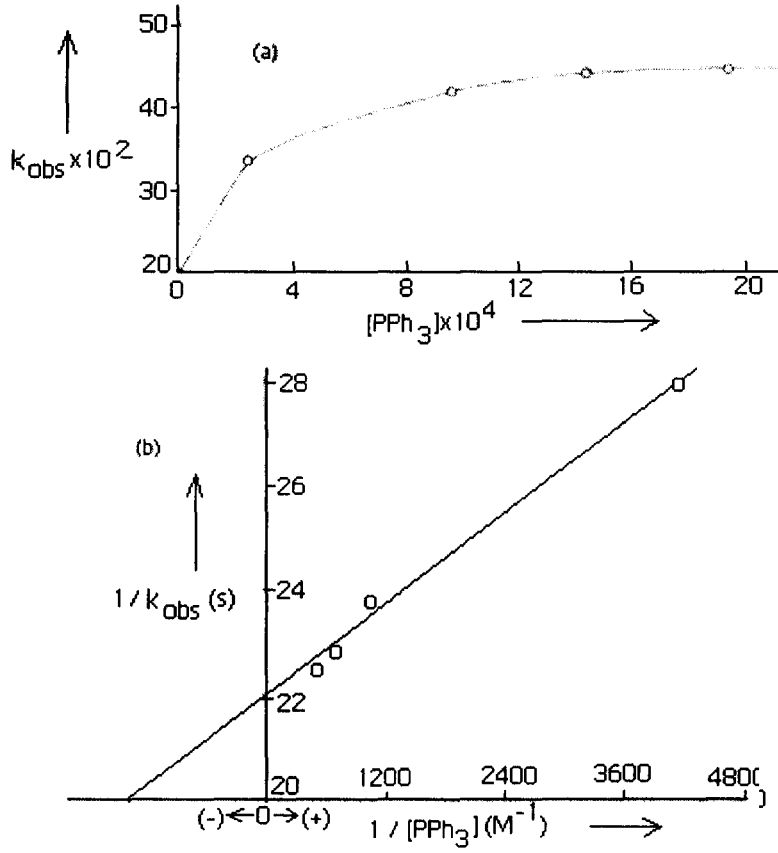

Fig.(III – 25):(a)Dependence of the rate of reaction of (**4**) [3.5x10 $^{-5}$(M)] with PPh_3 in DMF at 301 K; (b) the corresponding double reciprocal plot.

Compound (**3**) undergoes aerial oxidation to give (**4**) , which has been isolated in the solid state and well characterized through different physico-chemical means, as discussed above. Formation of (**4**) indicates the following reaction stoichiometry [steps 2(a) and 2(b) leading to overall reaction, as shown in (2)] as well as Scheme (III-3).

$$2 \text{ x comp.(3) } (Mo^{IV}) + O_2 \text{ (air)} \longrightarrow 2\,[Mo^{VI}O]^{4+} \text{complex} \text{ --- } 2(a)$$

$$2\,[Mo^{VI}O]^{4+} + H_2O \longrightarrow [Mo^{VI}_2O_3]^{6+} \text{complex} + 2H^+ \text{ --- } 2(b)$$

The overall reaction :

$$2 \text{ x comp.(3), } (Mo^{IV}) + O_2(air) + H_2O \longrightarrow \text{compound (4), } (Mo^{VI}_2O_3)^{6+}$$

$$\text{complex} + 2H^+ \text{ --(2)}$$

Similar to oxidation of (**2**) above (equation 1), moisture from atmosphere takes part in the second step oxidation of $[Mo^{VI}O]^{4+}$ core to $[Mo^{VI}_2O_3]^{6+}$ core [19, 20(c,d)], leading to the formation of compound (**4**) [36] [Equation (2)].

To complete the redox cycle, (**4**), so isolated above, was treated with slight excess of PPh_3, an oxygen abstractor, whereby the Mo^{VI} – atom in (**4**) undergoes reduction to the lower oxidation state (Mo^{IV}) as is present in (**3**) [Scheme (III - 3).

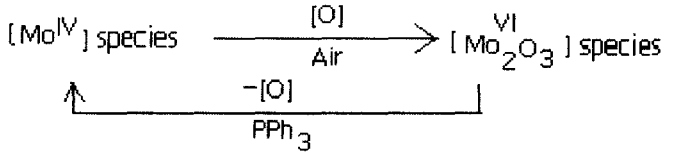

[Scheme (III - 3)]

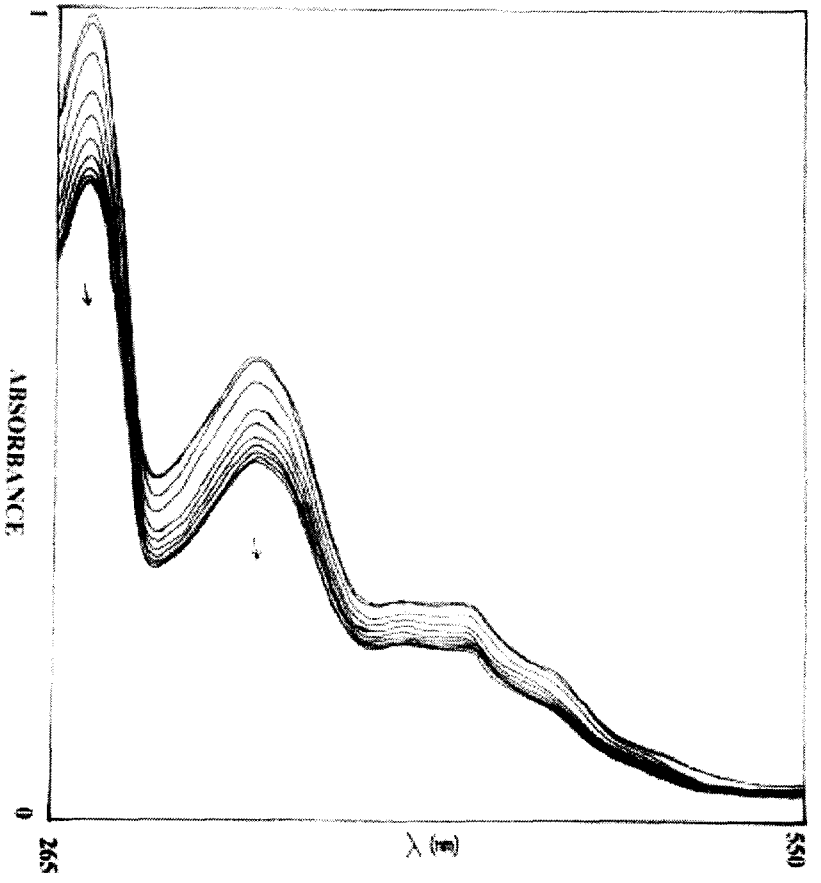

Fig. (III–26): UV–VIS absorption spectral changes recorded every 15 min. during the reaction of (**5**) [$2.05x10^{-5}$(M)] with $Me_3N\rightarrow O$ [$2.40x10^{-3}$(M)] in DMF at 301K.

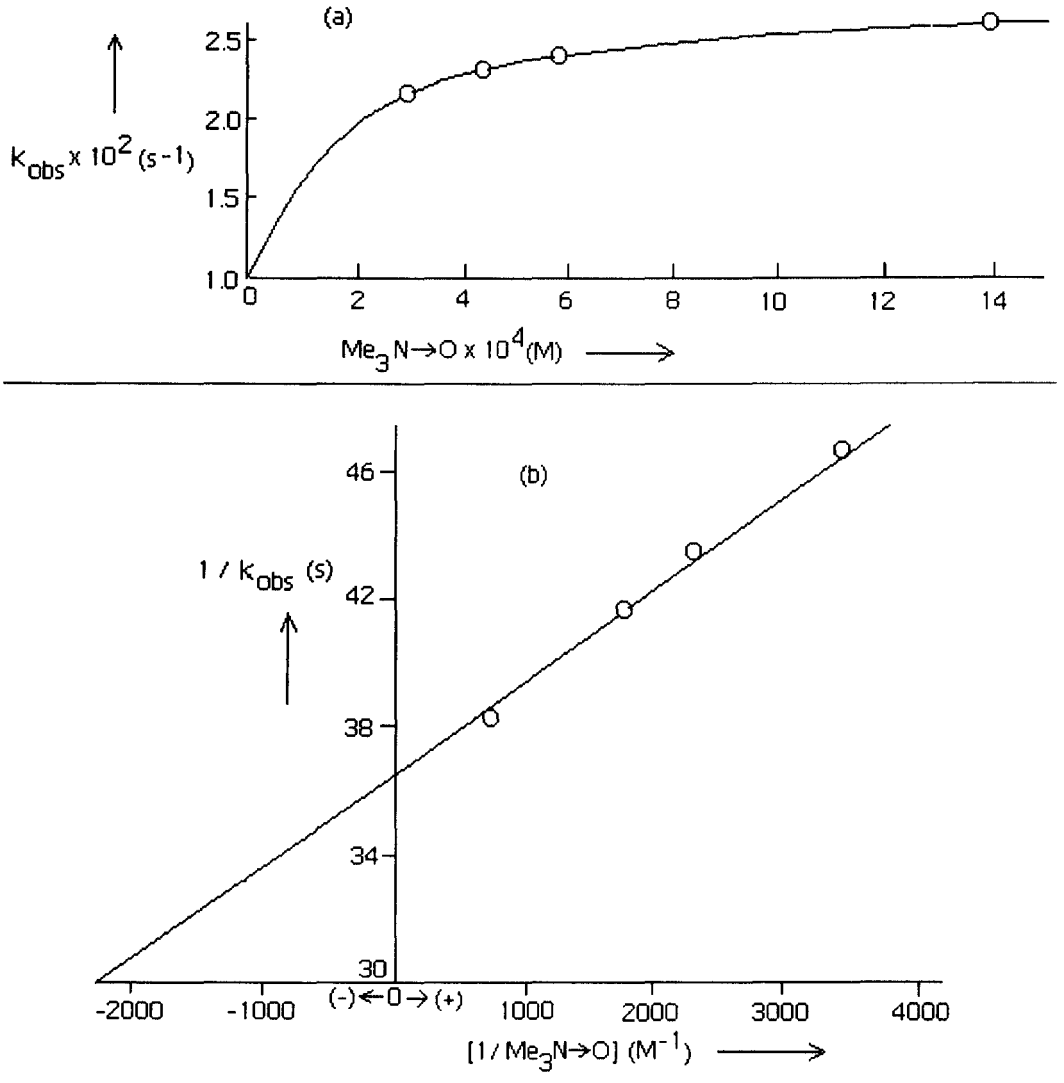

Fig.(III – 27):(a)Dependence of the rate of reaction of (**5**) [1.96x10 $^{-5}$(M)] with $Me_3N\rightarrow O$ in DMF at 301 K; (b) the corresponding double reciprocal plot

Here one thing should be noted that both (**3**) & (**4**) are quite stable under atmospheric condition although they contain different oxidation states of molybdenum. This stability of the molybdenum complexes in different oxidation states is due to the unique chelating effect of $H_3(pte_2\text{-}tsc)$ ligand. The overlay UV-VIS spectral change for the reaction of (**4**) with PPh_3 shows an isobestic point at 372 nm [Fig.(III–24)] suggesting a definite course of this conversion.

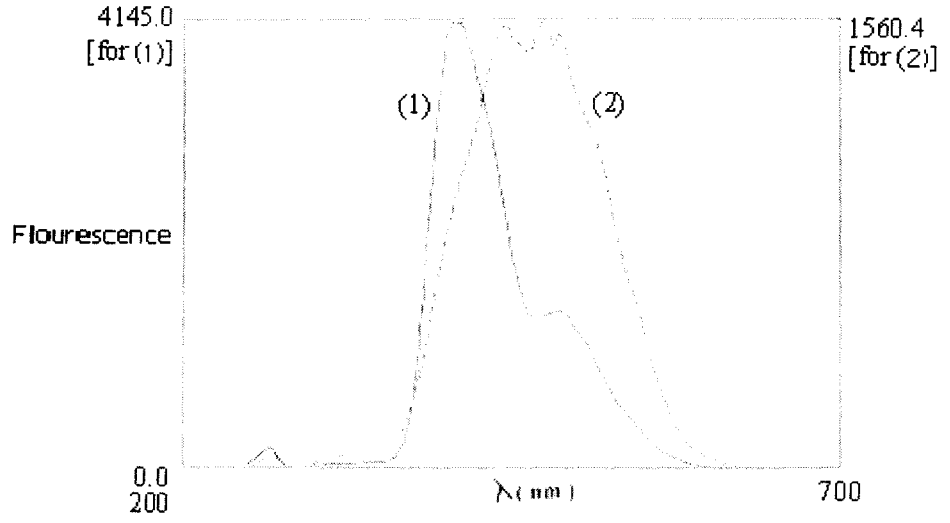

Fig.[III–28(a)]: Fluorescence spectra in DMF of (**5**)[$1.0x10^{-4}$(M)], curve (1) for the complex & curve (2) for its oxidized product after reaction with $Me_3N \rightarrow O$ in DMF.

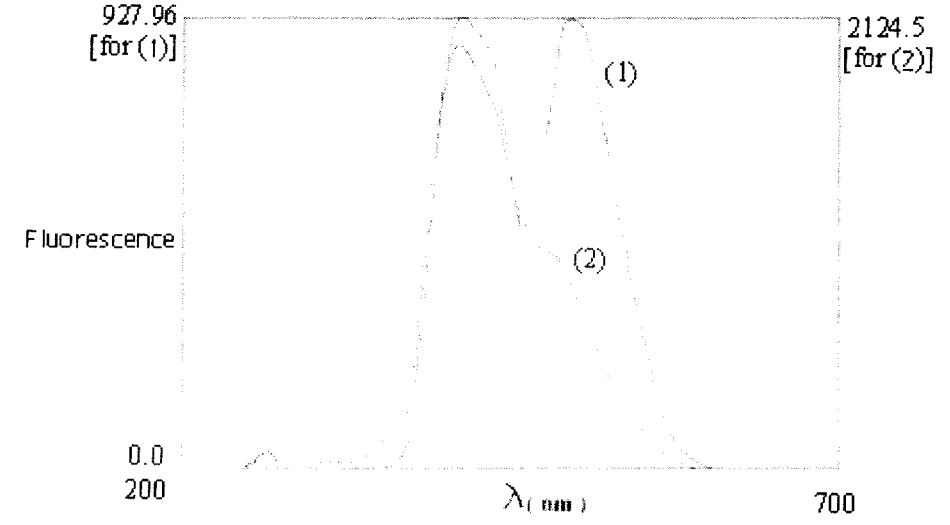

Fig.[III–28(b)]: Fluorescence spectra in DMF of (**7**) [$1.0x10^{-4}$(M)], curve (1) for the complex & curve (2) for its reduced product after reaction with PPh_3 in DMF.

To establish reaction stoichiometry of the reaction between (**5**) and $Me_3N{\rightarrow}O$, a DMF solution (60 ml) of (**5**) (1.87 g, 1 mmol) was allowed to react with $Me_3N{\rightarrow}O$ (0.75 g, 10 mmol) in the dark under a slow flow of N_2 gas, at 298 K for the first 24 h and then at 333 K for the next 24 h. The emerging gas carrying Me_3N (b.p. 275.9 K) was passed into a flask containing a measured excess of standard perchloric acid dissolved in glacial acetic acid and then the gas was released to the atmosphere through a silicone oil bubbler. Finally, the residual perchloric acid in the flask was back titrated potentiometrically using a standard sodium acetate solution [47] and the amount of perchloric acid consumed by Me_3N was estimated. About 3.2 mol of Me_3N was recovered per mol of (**5**) added, indicating a reaction represented by equation (3), below and supported by kinetic data.

$$[(Mo^{V}{}_2O)_2]^{16+} + 2\,Me_3N{\rightarrow}O \longrightarrow 4\,[Mo^{VI}O]^{4+}\ \text{complex} + 2\,Me_3N \quad \text{---- 3(a)}$$

$$2[Mo^{VI}O]^{4+}\ \text{complex} + Me_3N{\rightarrow}O + H_2O \longrightarrow 2[(Mo^{VI}O_2)]^{2+} + Me_3N + 2H^{+} \quad \text{--- 3(b)}$$

$$2[Mo^{VI}O]^{4+}\ \text{core} + 8Cl^{-}\ [\text{from}(\mathbf{5})] + \text{bipy}\ [\text{from}(\mathbf{5})] \longrightarrow [(Mo^{VI}OCl_4)_2(\text{bipy})] \quad \text{--- 3(c)}$$

The overall reaction :

$$\text{Compound } (\mathbf{5}) + 3Me_3N{\rightarrow}O + H_2O \longrightarrow 2[(Mo^{VI}O_2)]^{2+} + 3Me_3N + [(Mo^{VI}OCl_4)_2(\text{bipy})] + 2H^{+} \quad \text{--- (3)}$$

H_2O used in equation 3(b) most probably came from moisture in the solvent and took part in the hydrolysis of $[Mo^{VI}O]^{4+}$ core [19, 20(c,d)].

The solution in the reaction flask was concentrated to dryness in rotary evaporator and the material so obtained was purified by flash chromatography; Et_2O was used for removing the excess of $Me_3N{\rightarrow}O$ and the oxidized complex was eluted in DMF – CH_3OH (9 : 1, v/v). The product, $[(Mo^{VI}O_2)\{H(pte_2\text{-}tsc)\}CH_3OH]$, was characterized through elemental analysis, ESIMS and other physico-chemical studies. Its IR spectrum contains ν(Mo=O) band at 945.1 cm^{-1}, characteristic of terminal ($Mo{=}O_t$) frequency[20]. There is no band corresponding to bridging (Mo – O_b – Mo) frequency. The inserted oxygen atoms are utilized in converting $[(Mo^{V}_2O)_2]^{16+}$ core to $2(Mo^{VI}O_2)^{2+}$ core along with the formation of $[(Mo^{VI}OCl_4)_2(bipy)]$ [as per Fig.(III-16), most likely the Mo-atoms bonded to the Schiff base ligands gave the $(Mo^{VI}O_2)^{2+}$ core and Schiff base containing product; while the other two Mo-atoms bonded to the bipyridyl molecule gave $[(Mo^{VI}OCl_4)_2(bipy)]$ as a side product] accompanied by one unit oxidation of each Mo^{V} atom [equation (3)].

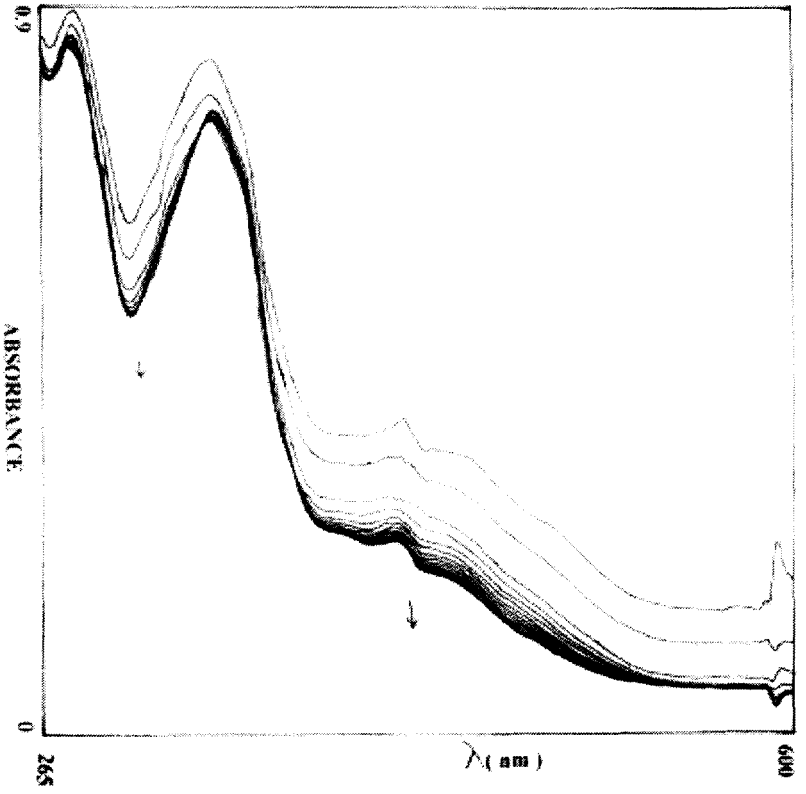

Fig.(III–29): UV–VIS absorption spectral changes recorded every 1 min. during the reaction of **(6)** [$3.40x10^{-5}$(M)] with $Me_3N{\rightarrow}O$ [$1.87x10^{-3}$(M)] in DMF at 301K.

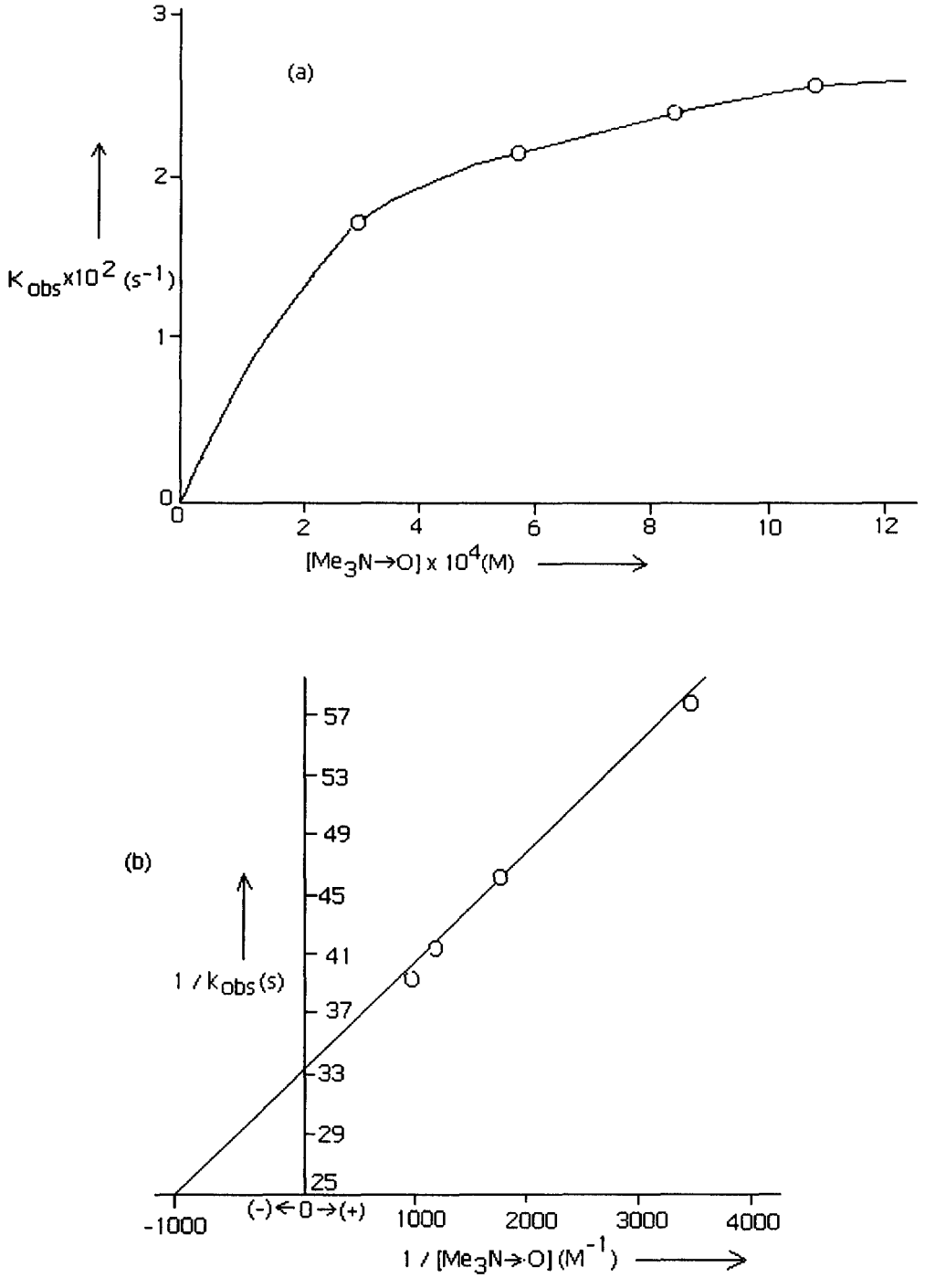

Fig.(III–30): (a)Dependence of the rate of reaction of **(6)** [3.14x10 $^{-5}$(M)] with $Me_3N\rightarrow O$ in DMF at 301 K; (b) the corresponding double reciprocal plot.

To establish reaction stoichiometry of (**7**) with PPh_3, a DMF solution (60 ml) of (**7**) (0.786 g, 1 mmol) was allowed to react with PPh_3 (2.62 g, 10 mmol) in the dark under a slow but steady flow of N_2 gas, at 298 K for the first 24 h and then at 333 K for the next 24 h. The solution in the flask was concentrated to dryness in rotary evaporator and the material so obtained was purified by flash chromatography; Et_2O was used to remove the excess PPh_3. The oxidized product $Ph_3P = S$, produced during the reaction was eluted in a mixture of CH_2Cl_2 – CH_3OH (1:1 v/v) (the metal complex is insoluble in this solvent mixture), evaporated to dryness and extracted in Et_2O to get 0.85 mol of $Ph_3P = S$ per mol of (**7**) added [90], supporting the reaction represented by equation (4), below and substantiated by kinetic data.

The reduced Mo–complex [equation (4)] was eluted in DMF - CH_3OH solvent mixture (2 :3 v/v); and characterized through elemental analysis, ESIMS and other physico-chemical studies. Its composition was found to be $[(Mo_2^{V}S_4)\{H(pte_2\text{-}tsc)\}(CH_3OH)_3].CH_3OH$. The oxygen atom containing counterparts of the $[Mo_2^{VI}S_5]^{2+}$ and $[Mo_2^{V}S_4]^{2+}$ core are well known, e.g., $[Mo_2^{VI}O_5]^{2+}$ and $[Mo_2^{V}O_4]^{2+}$ cores [2, 19]. Compound (**7**) has formula weight of 787, whereas, ESIMS spectrum of this reduced complex shows peak at m/z = 754 [Fig.(III–31e)] giving a difference of 33 mass unit (787 – 754 = 33) corresponding to the loss of one S atom from (**7**) by PPh_3 accompanied by the release of one H atom [85, 107]. This peak is simulated by using the IPC computer program [46] at m/z = 754 [Fig.(III-31f)]. [Fig.(III–31a)] represents the ESIMS peaks of (**7**) at m/z = 760, $[M - CO + H]^+$ and its computer simulation result [Fig.(III–31b)]; [Fig.(III–31c)] represents the experimentally found peaks in the reduced product, at m/z = 728, $[M - (CO + S) + H]^+$ corresponding to the loss of one S atom from that in Fig.(III–31a) [760 – 728 = 32 mass unit].

(Comp.**7**), $[(Mo_2^{VI}S_5]^{2+}$ + PPh_3 ⟶ $[(Mo_2^{V}S_4]^{2+}$ core containing complex

+ Other products e.g., $Ph_3P = S$, CH_3OH etc.--- (4)

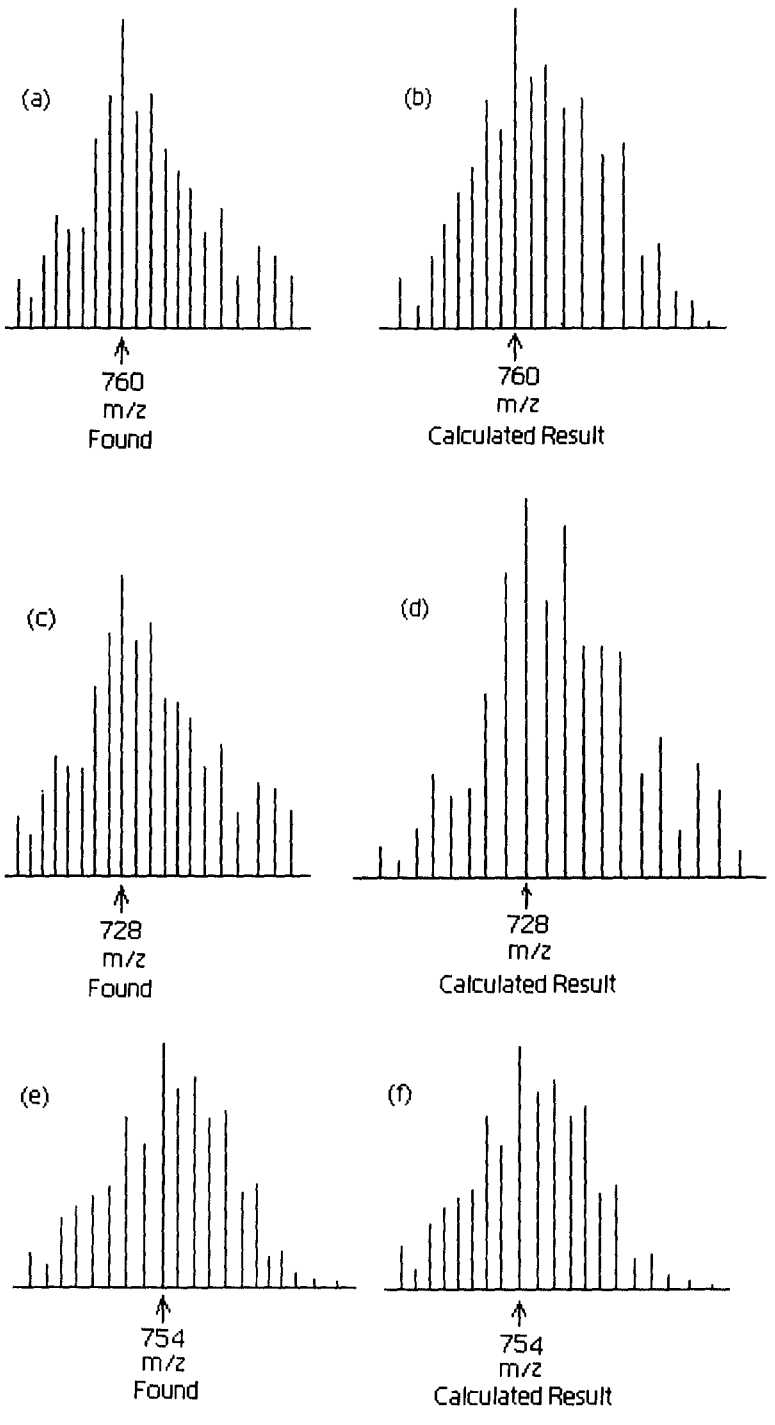

Fig.(III–31): (a) Experimentally found and (b) computer simulation peaks of (7) corresponding to m/z = 760,$[M - CO + H]^+$, formula- $C_{13}H_{28}N_8O_5Mo_2S_6$; (c) experimentally found and (d) computer simulation peaks of the product obtained after reduction of (7) by PPh_3, corresponding to m/z = 728, $[M - (CO + S) + H]^+$, formula- $C_{13}H_{28}N_8O_5Mo_2S_5$; (e) experimentally found and (f) computer simulation peaks of the product obtained after reduction of (7) by PPh_3, corresponding to m/z = 754, $[M - S - H]^+$, formula- $C_{14}H_{26}N_8O_6S_5Mo_2$.

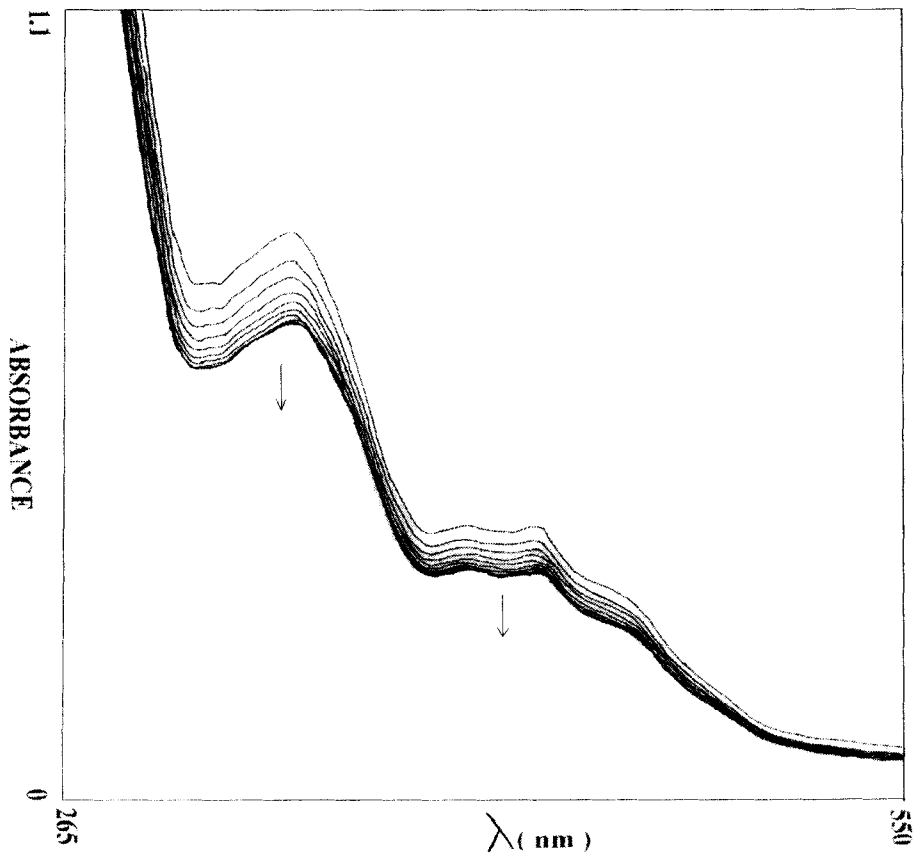

Fig.(III–32): UV–VIS absorption spectral changes recorded every 12 min. during the reaction of (7) [$1.1x10^{-5}$(M)] with PPh_3 [$1.46x10^{-3}$(M)] in DMF at 301K.

As these compounds (**2–7**) undergo oxygen atom transfer reaction with PyN→O, Me_3N→O / PPh_3 ; kinetics of these reactions were followed spectrophotometrically at 400 nm for (**2**), 420 nm for (**3**), and at 415 nm for compounds (**4 – 6**) and in case of (**7**), kinetics studied at 510 nm. Rate constants were measured at room temperature as well as at three different higher temperatures by applying least square method and ploting $\log(A_t - A_\infty)$ or $\log(A_\infty - A_t)$ vs time for the decay or growth kinetics for (**2, 3, 5, 6**) and (**4 & 7**) respectively. At room temperature the k_{obs} (s^{-1}) values were measured at different complex : substrate ratio and when plotted as a function of substrate concentrations, substrate saturation plots were obtained [Fig.s (III–21a), (III–23a), (III–25a), (III–27a), (III–30a) & (III–33a)]. Double reciprocal plots were obtained from the substrate saturation kinetic data by ploting $1/k_{obs}$ vs. 1/[substrate] for

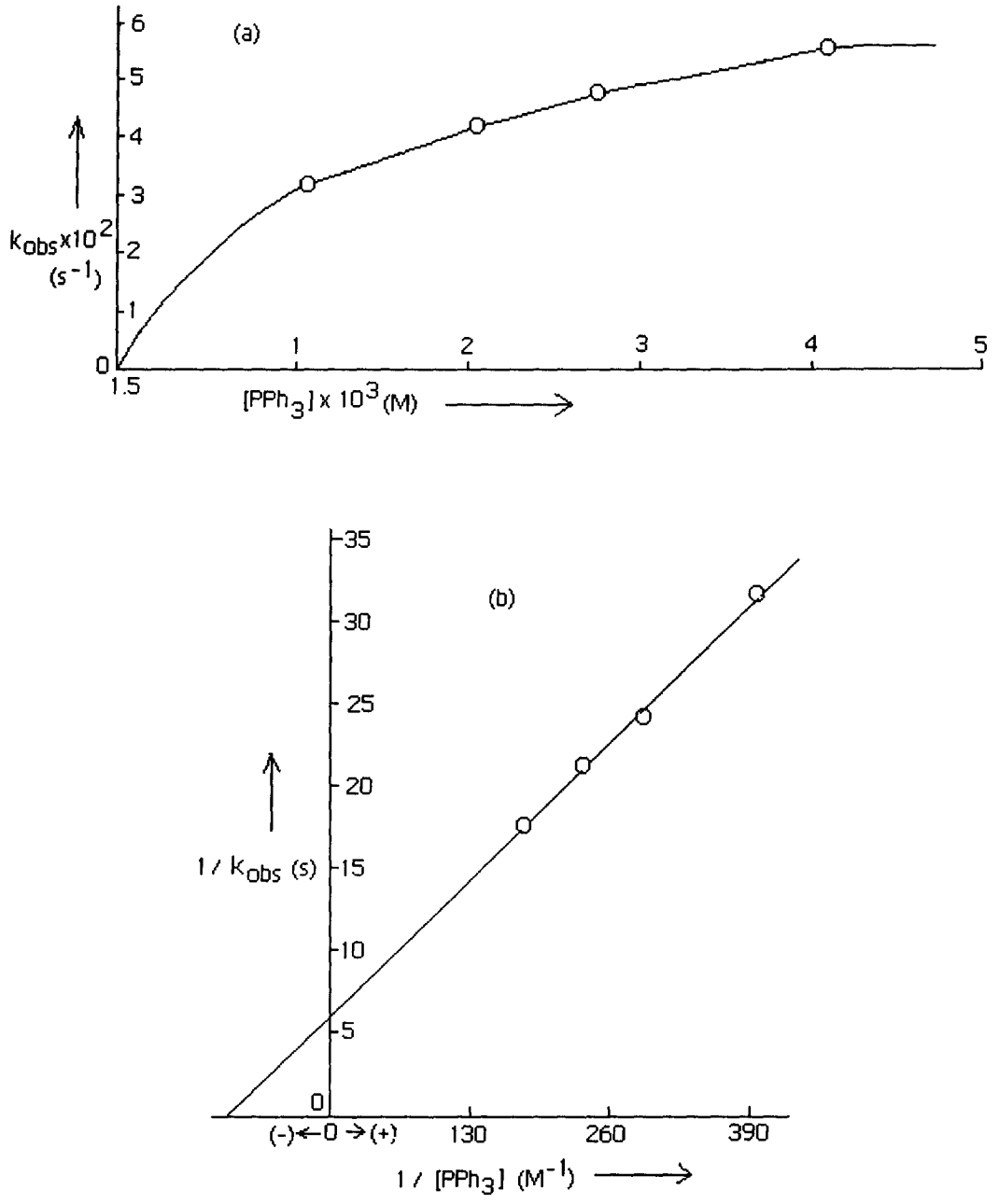

Fig.(III–33): (a)Dependence of the rate of reaction of (7) [$2.28x10^{-4}$(M)] with PPh_3 in DMF at 301 K; (b) the corresponding double reciprocal plot.

each complex [Fig.s (III–21b), (III –23b), (III–25b), (III–27b), (III–30b) & (III–33b)]. K_M and k_2–values [Table (III – 15)] were calculated from the slops and intercepts of these straight line plots respectively.

Now, for measuring activation parameters, four different k_{obs} (s^{-1}) values corresponding to four different reaction temperatures were measured for each complex, at the pseudo – first order substrate saturation composition (substrate concentration, 35–70 times excess to that of the complex) [8(a,c), 17, 23]. Arrhenius and Eyring plots were obtained from the temperature dependent rate constant values, by ploting $\ln(k_{obs})$ vs. $(1/T)x10^3$ and $\ln(k_{obs}/T)$ vs. $(1/T)x10^3$ respectively. From the slope of Arrhenius plots activation energy (E_a–value) is calculated [Table (III–15)]. Other activation parameters, $\Delta H^{\#}$ and $\Delta S^{\#}$ - values are obtained from slope and intercept of the Eyring plots respectively. $\Delta G^{\#}$-values are calculated from the Gibb's–Helmholtz equation, $\Delta G^{\#} = \Delta H^{\#} - T\Delta S^{\#}$ [Table (III–15)].

The overlay scan during spectrophotometric monitoring of the oxygen atom transfer reactions of (**2**), (**3**), (**5**) and (**6**) with PyN→O or Me_3N→O show decay kinetics (i.e., lowering of OD value with time), whereas the reverse is true (growth kinetics) for the reaction of (**4**) with PPh_3. That is metal – centered oxidation is associated with decay kinetics and the reduction process shows a growth kinetics. The only exception to this general observation is compound (**7**), where sulphur atom abstraction (by PPh_3) takes place instead of oxygen atom transfer reaction. Most likely greater polarisability of the thiomolybdate core is responsible for this decay kinetics observed here; the same factor may be responsible for the failure of the $H_3(pte_2\text{-}tsc)$ ligand to reduce the metal centre (to V or IV state) during the synthesis of (**7**).

Table (III – 15)

Comp -ound No.s	Substrate used (in DMF)	T (K)	k_{obs} (s^{-1}) x 10^3	k_2 (s^{-1}) x 10^3	K_M (M) x 10^5	E_a (KJ, mol^{-1})	$\Delta H^{\#}$ (KJ, mol^{-1})	$\Delta S^{\#}$ (J,mol^{-1}, deg^{-1})	$\Delta G^{\#}$ (KJ, mol^{-1})
(2)	PyN→O	298 304 307.5 312	3.82 7.16 10.12 15.10	9.97	11.9	75.99	74.40	-208.29	137.73
(3)	Me_3N→O	300.5 307 311.5 315	21.70 26.00 29.00 32.00	25.4	19.9	21.30	17.92	-202.40	78.75
(4)	PPh_3	307 312 316 318	44.50 58.40 73.00 80.00	45.6	6.57	43.11	41.88	-205.00	104.83
(5)	Me_3N→O	302 305.5 314 318	26.10 27.40 31.70 33.60	27.4	8.0	12.76	10.21	-200.4	70.64
(6)	Me_3N→O	302 308.5 313 318	25.50 26.80 27.60 28.60	30.3	21.5	5.78	3.18	-198.63	63.12
(7)	PPh_3	291 295.5 302.5 308.5	56.60 59.50 65.40 71.00	171.4	1100	9.95	7.09	-200.40	67.72

$$k_{obs} = k_2[S]/(K_M + [S]) \quad \text{---- (5)}$$

Where, $K_M = (k_2 + k_{-1})/k_1$,

Or,

$$1/k_{obs} = 1/k_2 + K_M/k_2[S] \quad \text{---- (6)}$$

Plots of k_{obs} vs. [S] indicates substrate saturation kinetics [Fig.s (III–21a), (III–23a), (III–25a), (III–27a), (III–30a) & (III –33a)] as per equation (5) above and plots of $1/k_{obs}$ vs $1/[S]$ gave straight lines, named as double reciprocal plots [Fig.s (III –21b), (III –23b), (III –25b), (III –27b), (III –30b) & (III –33b)] as per equation (6); with slope equal to K_M/k_2 and intercept equal to $1/k_2$. The kinetic parameters for the above reactions along with k_{obs}, k_2 & K_M values are presented in Table (III – 15) and they found to be in good agreement with the available literature on molybdenum complex mediated oxygen atom transfer kinetics data [8, 17, 23].

One interesting observation from the kinetic measurement [Table(III–15)] is that the entropy of activation ($\Delta S^{\#}$) value is found to be negative for all the reactions studied here. This is in conformity with the associative type of reaction mechanism, alike to enzyme – substrate type reaction mechanism [24, 34]. The variation in the magnitude of the kinetic parameters in Table-(III–15) can be understood in terms of several factors, e.g., the steric energy of the foregoing CHEM3D representations, metal atom oxidation states, steric crowding around the metal centre etc. High k_{obs} values are obtained in cases involving oxygen or sulphur abstraction by PPh_3. As a substrate, $Me_3N{\rightarrow}O$ provides higher k_{obs} values than $PyN{\rightarrow}O$. Higher E_a (activation energy) value is observed for (**2**) where the ligand coordination around the Mo^{IV} centre is most compact, with lowest steric energy (for CHEM3D representations). Reactivity of compound (**6**) can also be viewed in the same light. Compounds with high steric energy usually show low E_a values with a few exceptions, indicating the responsibility of other factors stated above in the reactivity process.

Cyclic voltammetry (CV) data, (a) from – 1.85 to 1.0 V is shown in one figure along with expansion of the region (b) – 0.2 to 0.9 V of the free ligand, $H_3(pte_2$-tsc) (**1**). This shows a quasi – reversible couple in the region – 0.85 V (reduction) and – 0.68 V (oxidation). ΔE_p ($E_{pc} - E_{pa}$ = 170 mV) value can be correlated essentially with a two – electron transfer process, taking into account the Nernst equation as well as the iR drop during the recording process. Presence of the 1,4 – diazine residue in the pterin ligand in conjunction with the 7-substituted side chain containing the thiosemicarbazide residue, imparts a degree of structural stability and availability of suitable orbitals makes this ligand stable enough during this 2-electron redox process without undergoing chemical decomposition on the CV time scale. These factors are responsible for the observed quasi-reversible behaviour in Fig.(III-34a) [4]. Two irreversible oxidation peaks at – 0.20 V and + 0.74 V characterize the rest part of this CV data [Fig.(III –34)].

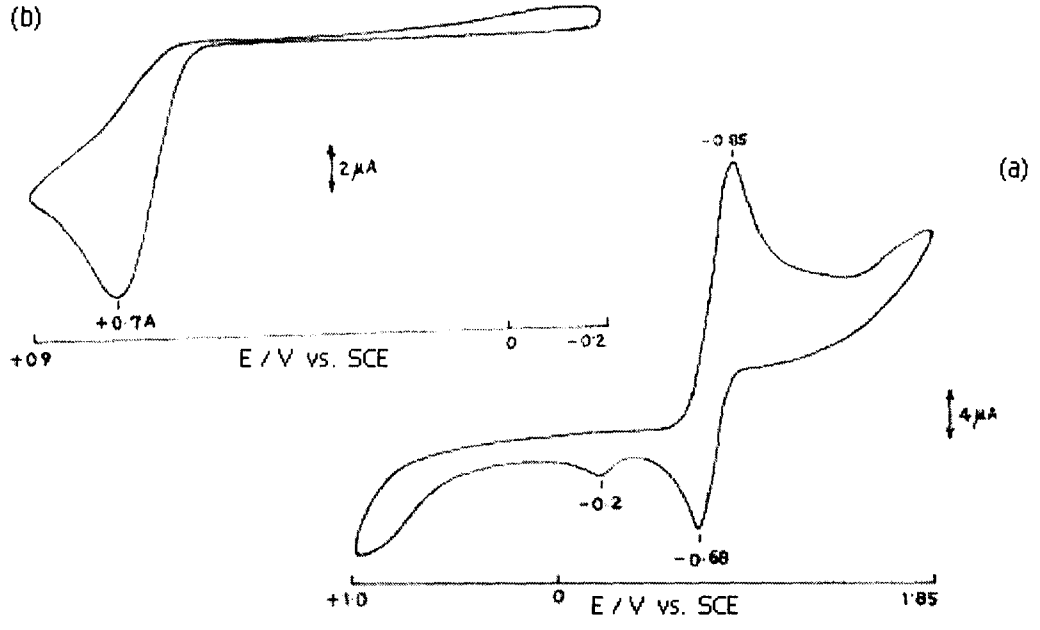

Fig.(III–34): CV scans of compound (**1**) [1.0 x 10^{-3}(M], Bu_4NClO_4 [0.1 (M)] in DMF, (a) – 1.85 to +1.0 V, (b) – 0.2 to +0.9 V. Scan rate 50 mVs^{-1}.

Fig. (III –35) shows the CV data of compound (**2**) which is characterized by the aforesaid quasi – reversible peak as well as additional peaks on (b) for the metal centre; at – 0.105 V a reduction of the metal – centre ($Mo^{IV} \rightarrow Mo^{III}$) takes place followed by chemical attack of the solvent leading to its partial decomposition. The quasi-reversible peak system in Fig.(III-35a) is essentially related to ligand redox process. A weak signal at + 0.45 V characterizes the reoxidation process of the metal – centre.

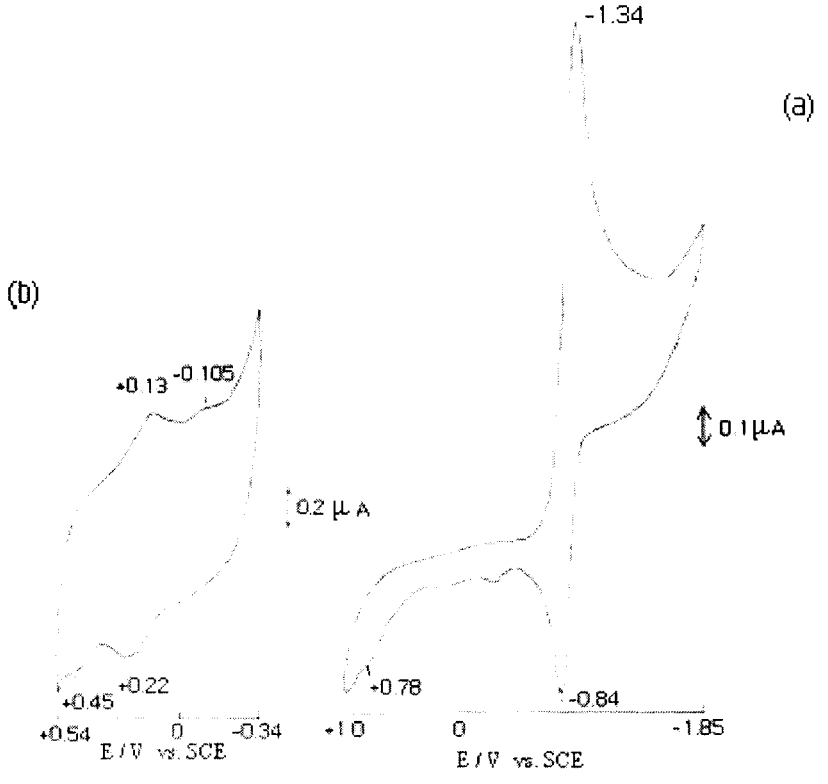

Fig.(III–35):CV scans of compound (**2**) [1.0x10 $^{-3}$ (M)], Bu_4NClO_4 [0.1 (M)] in DMF, (a) – 1.85 to – 1.0 V, (b) – 0.34 to + 0.54 V. Scan rate 50 mVs^{-1}.

In case of (**3**), in addition to the above mentioned common features the metal irreversible reduction peak ($Mo^{IV} \rightarrow Mo^{III}$) is observed at – 0.43 V and the subsequent reoxidation step at + 0.53 V. In case of complex (**4**), the metal – centers undergo reduction ($Mo^{VI} \rightarrow Mo^{V}$) at + 0.15 V and subsequent reoxidation occurs at + 0.24 V. The ΔE_p value for the ligand reduction peak corresponds to essentially one electron transfer (taking into account the iR drop aspect). One additional irreversible ligand reduction peak appears at – 1.34 V. CV data of compound (**5**) is characterized

essentially by similar features as above with the metal reduction ($Mo^{V} \rightarrow Mo^{IV}$) preak appearing at +0.16 V and the subsequent reoxidations occurring at – 0.17 V, + 0.22 V & + 0.49 V respectively. For compound (**6**) the metal reduction ($Mo^{V} \rightarrow Mo^{IV}$) peak is observed at +0.13 V and the subsequent reoxidation occurs at + 0.47 V. In case of (**7**), [Fig.(III–36)], the metal reduction ($Mo^{VI} \rightarrow Mo^{V}$) takes place at – 0.26V. Besides this the ligand part is characterized by essentially an irreversible system as opposed to quasi – reversible behavior here; possibly the highly polarizable thiomolybdate residue of this complex is responsible for this behavior.

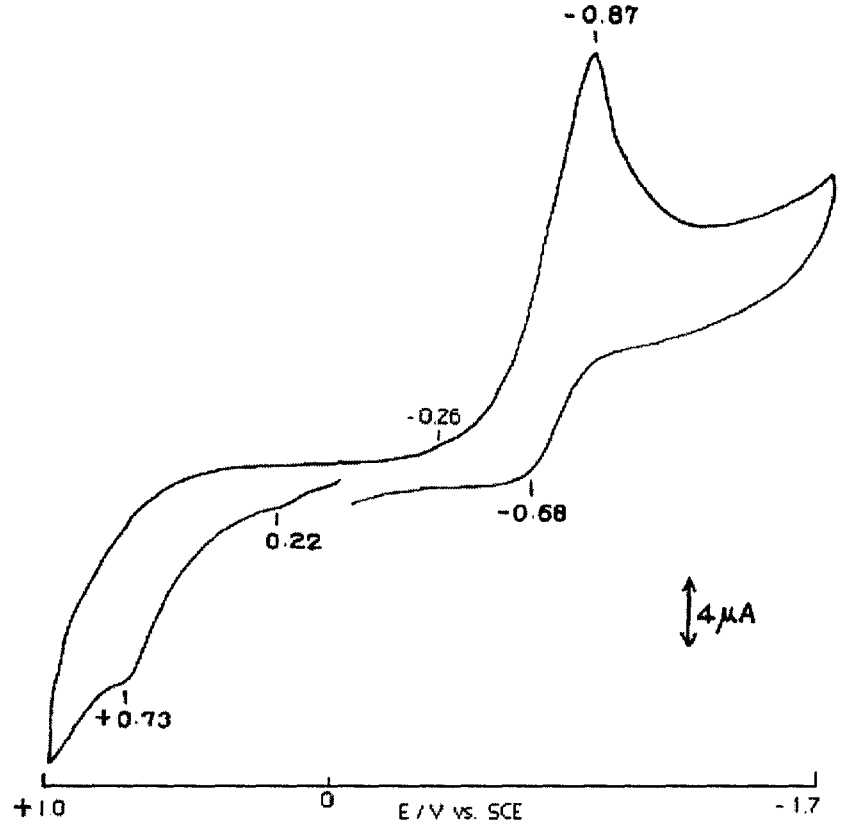

Fig.(III– 36): CV scans of compound (7) [1.0×10^{-3} (M)], Bu_4NClO_4 [0.1 (M)]in DMF. Scan rate 50 mVs^{-1}.

It may be summarized that both the ligand residue as well as the metal centre take part in the overall redox activity of these complexes.

Conclusion

Here the synthesis and characterization of a new Schiff base ligand are described along with its six new complex compounds of molybdenum in different oxidation states. In most cases the pterin ligand acts as a reducing agent during synthesis and oxidation state of the metal centre in the final product depends on the reaction condition used as well as the nature of the molybdenum starting material. ESIMS data in conjunction with elemental analysis data and supported by IR and ^{1}H NMR spectral studies, verify their **formulations / chemical compositions**. Molecular modeling studies [CHEM3D models obtained through MM2 calculations] provide with their optimized molecular geometry as well as bond length and bond angle data. The later type of parameters are in agreement with the published X-ray structural data on different molybdenum – pterin coordination compounds in related systems. This aspect verifies their **molecular structures**. Reactivities of these compounds towards oxygen donors ($Me_3N\rightarrow O$ / $PyN\rightarrow O$) or oxygen abstractor (PPh_3) throw light on the **oxidation state of the metal centre** in these compounds. The k_{obs} (s^{-1}) values are within the range of oxygen atom transfer reactions of related published synthetic $Mo^{IV\,/\,VI}$ – systems. Nature of such group transfer reactions has been substantiated by **reaction stoichiometry studies** in several cases as well as ESIMS data in one case. Almost all these cases conform to **substrate saturation type kinetics** with **negative entropy of activation** value ($\Delta S^{\#} = -198$ to -208 J $mol^{-1}deg^{-1}$).

CV data as well as fluorescence spectral data throw light on the **changes in electronic structure during different redox steps** described in this chapter. It is evident that the ligand centred as well as the metal centred redox systems supplement each other in the present new molybdenum compounds, giving them unique oxygen atom transfer reactivity towards typical enzyme substrates of oxomolybdoenzymes. In this sense, they can be considered as **functional model systems**. UV-VIS as well as **fluorescence spectra** have proved to be **valuable probes** for **studying this aspect**.
